Chromosome territory relocation during DNA repair requires nuclear myosin 1 recruitment to chromatin mediated by ϒ-H2AX signaling

Mugdha Kulashreshtha[1], Ishita S. Mehta[1,2], Pradeep Kumar[1,2] and Basuthkar J. Rao[1,*]

[1]Department of Biological Sciences, Tata Institute of Fundamental Research, Mumbai, Maharashtra 400005, India and [2]UM-DAE Centre for Excellence in Basic Sciences, Biological Sciences, Kalina Campus, Santacruz (E), Mumbai, Maharashtra 400098, India

ABSTRACT

During DNA damage response (DDR), certain gene rich chromosome territories (CTs) relocate to newer positions within interphase nuclei and revert to their native locations following repair. Such dynamic relocation of CTs has been observed under various cellular conditions, however, the underlying mechanistic basis of the same has remained largely elusive. In this study, we aim to understand the temporal and molecular details of such crosstalk between DDR signaling and CT relocation dynamics. We demonstrate that signaling at DNA double strand breaks (DSBs) by the phosphorylated histone variant (ϒ-H2AX) is a pre-requisite for damage induced CT relocation, as cells deficient in ϒ-H2AX signaling fail to exhibit such a response. Inhibition of Rad51 or DNA Ligase IV mediated late steps of double strand break repair does not seem to abrogate CT relocation completely. Upon DNA damage, an increase in the levels of chromatin bound motor protein nuclear myosin 1 (NM1) ensues, which appears to be functionally linked to ϒ-H2AX signaling. Importantly, the motor function of NM1 is essential for its recruitment to chromatin and CT relocation following damage. Taking these observations together, we propose that early DDR sensing and signaling result in NM1 recruitment to chromosomes which in turn guides DNA damage induced CT relocation.

INTRODUCTION

Both endogenous as well as exogenous DNA damage can lead to genomic instability and may even be lethal if they are not repaired accurately and timely. When faced with DNA damage, cells generally respond by a two-step strategy: cells undergo cell cycle arrest and try to repair them (1,2), but if the damages are too severe to be repaired, apoptosis is induced leading to cell death (3,4).

Double strand breaks (DSBs) in the DNA can be repaired by two major repair pathways namely – the non homologous end joining (NHEJ) or homologous recombination (HR) (5,6). DSBs are sensed by ATM kinase, which in turn gets activated and phosphorylates a number of downstream protein targets that participate in the DSB repair pathways (7). One such phosphorylation target of ATM kinase is H2AX (8), a histone H2A variant that represents about 2–25% of the H2A complement in the genome (9). H2AX present in the chromatin, flanking a DSB, gets phosphorylated at its Ser139 residue in mammalian cells also by several other members of the phosphatidylinositol 3-kinase-like kinases (PI3KK) family, such as ATR, DNAPK (8,10) and the phosphorylated version of H2AX is referred to as ϒ-H2AX (9). Once formed ϒ-H2AX via downstream signaling leads to the recruitment of ATM kinase at the DSB sites, ultimately resulting in the formation of more ϒ-H2AX molecules in the chromatin, thereby generating an important 'hub' of protein–protein interactions required for DNA repair (11,12). Such ϒ-H2AX foci spanning up to 1 Mb can form on either side of the break (9,13) and signal the recruitment of several repair proteins such as MDC-1, RNF8/UBC13, 53BP1, BRCA1, etc. (14,15) and chromatin modifiers such as IN080 and NuA4 to the DSBs (16–18). As expected, H2AX deficient cells are hypersensitive to DNA damage and show defective cell cycle checkpoint activity (19–21). In such cells, DSB repair by HR is inefficient even though the NHEJ repair pathway seems to be unaffected (22).

In yeast, DSBs have been shown to cause increased local mobility of chromatin, which is implicated in enhancing the search for homology, thus leading to HR based repair (23,24). Such enhanced mobility in chromatin is known to require active repair proteins such as Mec1 (ATR homolog) and HR proteins like Rad51, Rad54 (25). In contrast, a study in mammalian cells has shown that DNA ends at a single targeted DSB appear to be positionally sta-

*To whom correspondence should be addressed. Tel: +91 22 22782606; Fax: +91 22 22804610; Email: bjrao@tifr.res.in

ble, which might attenuate illegitimate joining of breaks, genomic instability and consequent inaccurate repair (26). Even though single DSBs are ascribed to be positionally stable, chromatin domains containing multiple random breaks seem to undergo spatial movements, which in turn depend on higher order organization of chromatin (27). Moreover, relocation of chromatin domains may also contribute to multiple DSBs clustering together at repair foci as observed in yeast and mammalian cells (28,29). Such dynamic clusters of repair foci are thought to represent repair centres or even factories (28–31).

In mammalian interphase cells, every chromosome occupies a specific position within the nucleus, referred to as chromosome territory (CT) (32–35). Such non-random arrangement of chromosomes within the nucleus has been studied in several different species such as humans, apes, chicken, bovine, etc. (34,36,37) and it has been found that the organization of the CTs is based on gene density, where the gene dense chromosomes position in the centre of the nucleus and the gene poor chromosomes toward the nuclear periphery (38,39). Several studies have shown that certain CTs relocate to new locations within the nucleus under specific conditions such as serum starvation, disease, differentiation, etc. (40–45). We have previously reported that certain CTs reposition in the nucleus in response to DNA damage induced by agents such as cisplatin and hydrogen peroxide that lead to production of DNA DSBs during DNA damage response (DDR) (46–54). Such DNA damage induced CT repositioning is dependent on sensing and repair of the damage (46). Previous studies have demonstrated that open chromatin and gene rich chromosomes are more susceptible to DNA damage (55,56). CT relocation following DNA damage seems to be somehow linked to the gene density status of the chromosomes since only the relatively gene-rich CTs show such damage induced relocation (46). DNA damage induced CT relocation spans over a distance of several microns similar to that of long-range clustering together of repair foci observed in mammalian cells (29,30). We surmise that radiation induced multiple damage containing chromatin domains from different CTs coalesce into repair centres (29,30), and this may be akin or mechanistically linked to the dynamic changes associated with damage induced CT relocations. Importantly, CT relocation is reversible upon repair, i.e. the CTs return to their 'native positions' after the damaging agent is removed and the cells are allowed to recover (46).

Nuclear motors such as actin and myosin have been shown to play an important role in the relocation of CTs following serum starvation (40) and also in the repositioning of a gene locus (57), or a chromosome site upon gene activation (58). Nuclear myosins are encoded by several classes of myosin genes including MYO1C that expresses three different protein isoforms – isoform A, isoform B or nuclear myosin 1 (NM1) and isoform C that get translocated into the nucleus via an NLS present in all the three isoforms (59–62). NM1 was the first nuclear myosin to be identified (63) and is the predominant nuclear isoform, whereas isoform C is primarily localized in the cytoplasm (60). Isoform C is the shortest isoform and differs from NM1 by the absence of 16 amino acids from the N-terminus of NM1 (59,60). The longest MYO1C gene encoded isoform is A, which was

identified recently by Ihnatovych *et al*. (60). Interestingly, nuclear isoforms A and B seem to have diverse functions as the former co-localizes only with Pol II, while the latter interacts with both Pol I and Pol II (60). NM1 and nuclear actin have been shown to function in transcription mediated by RNA polymerase I and II (64–71). It was discovered as early as 2004 that an actomyosin motor complex is physically coupled to RNA pol I machinery (72), but it is only recently that the direct interactions of NM1 with rDNA chromatin and Pol II promoters were demonstrated using ChIP/qPCR and ChIP Seq techniques (69,70,73). Moreover, these studies have shown that NM1 interacts with rDNA through its C-terminus, which in turn is regulated by GSK3β mediated phosphorylation of NM1 (69,73). Such chromatin bound NM1 functions together with RNA Pol I-associated actin to regulate rDNA transcription (66,69). NM1 also participates in chromatin remodeling through interactions with WSTF and SNFh2 components of the B-WICH remodeler complex (64,69). Almuzzaini *et al*. have also provided insights about how NM1 helps in the maintenance and preservation of Pol II activating histone modifications such as H3K9Ac and H3K4me3 by directly recruiting histone acetyl transferase PCAF and histone methyl transferase Set1/Ash2 to the chromatin (70).

Despite the extensive mechanistic knowledge of DDR pathways and nuclear motor protein functions in transcription, it is still unclear if and how DDR signaling, nuclear motor proteins are involved in DNA damage induced CT relocation. Here, using cisplatin as an inducer of DNA damage, we report that the early signaling by ϒ-H2AX is required for the repositioning of CTs within the nucleus following DNA damage. Later stages of repair catalyzed by proteins such as DNA ligase IV and Rad51 do not seem to play as critical a role as early sensors in programming the CT relocation events. We have also found that recruitment of the nuclear motor protein NM1 to chromatin increases after cisplatin or hydrogen peroxide induced DNA damage; which seems to be functionally coupled with ϒ-H2AX signaling and dependent upon the sensors of DNA damage such as ATM, ATR, PARP-1 and DNAPK. Knocking down of NM1 levels by RNAi or motor function defects in NM1 also lead to the failure of CT relocation during DDR. All these results put together, for the first time, suggest that early events of DDR and the DNA damage induced NM1 recruitment to chromosomes drive the spatial changes in CTs following DNA damage.

MATERIALS AND METHODS

Cell culture, treatments

Early passage Normal Human Dermal Fibroblasts (NHDFs) from Sigma-Aldrich were cultured in Dulbecco's Modified Eagl's Medium (DMEM) supplemented with 15% fetal bovine serum (FBS), 200 mM glycine and 1X antimycotic antibiotic (Gibco).

For inducing DNA damage, cells were treated with 25 μM cisplatin (Calbiochem) for 4 h. H_2O_2 treatment was carried out with 1 mM H_2O_2 for 90 min. Cells were treated with 10 μM of ATM (KU55933), ATR (Inhibitor IV/VE821), DNAPK (Inhibitor II/NU7026) or PARP (Inhibitor III/DPQ) (all from Calbiochem) for 1 h. DNA ligase

IV inhibition was done by treating cells with 1 μM SCR7 (kindly provided by Prof. Sathees C. Raghavan, Indian Institute of Science) for 24 h. LiCl was added to cells at a concentration of 20 mM for 3 h for inhibiting GSK3β kinase. All damage or inhibitor treatments were performed at 37°C.

Plasmid constructs and transfections

FLAG tagged wild-type H2AX and H2AX S139A mutant constructs (kindly provided by Prof. Junya Kobayashi, Kyoto University) were transfected into NHDFs using lipofectamine 2000 (Life technologies) and stable cells were selected 48 h post transfection using 1 mg/ml of the antibiotic G418 for 1 week followed by ∼0.5 mg/ml G418 for at least 6–8 weeks. The imposed selection leads to about 40–50% of cells as FLAG positive in the population.

For experiments involving motor defective form of myosin protein, V5 tagged nuclear myosin constructs—wild type and G126S (motor function mutant) (kindly provided by Prof. Ingrid Grummt, German Cancer Research Centre) were over-expressed in NHDFs and stable cells were selected using G418.

RNAi

For Rad51 knock down studies, Rad51 siRNA from Dharmacon (ON-TARGETplus SMARTpool-Human RAD51 L-003530-00-0005) and control siRNA from Sigma (MISSION® siRNA Universal Negative Control #1) were used. A total of 100 nM of these siRNAs were transfected into cells using lipofectamine 2000 (Life Technologies) and samples were collected at 72 h post transfection.

For nuclear myosin knock down experiments, 100 nM of MYO1C siRNA from Dharmacon (ON-TARGETplus SMARTpool-Human MYO1C L-015121-00-0005) and control siRNA 5′-UUCUCCGAACGUGUCACGU-3′ were used (74). Since MYO1C siRNA is a mixture of oligonucleotide probes directed against entire MYO1C gene, the siRNA effects are not specific to any particular isoform of myosin 1C. siRNAs were transfected into cells using lipofectamine 2000 (Life Technologies) and samples were collected at 48 h post transfection.

Immunofluorescence assay

Cells were grown on coverslips and following cisplatin damage, cells were fixed with 4% PFA (1X PBS) for 10 min, permeabilized with 0.1% Triton X-100 (1X PBS) for 15 min. Cells were then incubated with antibodies to ϒ-H2AX (Abcam), 53BP1 (Santacruz), FLAG (Abcam) or Nuclear myosin1β [for detecting NM1] (Sigma) dissolved in 1% BSA (1X PBS) for an hour, followed by washes in 1X PBS and incubation with Alexa secondary antibodies (Invitrogen)(dissolved in 1% BSA) for 45 min. The coverslips were washed again in 1X PBS and stained with DAPI in Vectashield mounting media. Cells were imaged using a Zeiss Axiovert 200 microscope.

Immuno-fluorescence *in situ* hybridization (Immuno-FISH)

Immuno-FISH was carried out using a previously published protocol (75). Briefly, cells were grown on slides and fixed with 4% PFA (1X PBS) for 10 min. The slides were then washed thrice in 0.05% Triton X-100 (1X PBS) for 5 min each time and cells were permeabilized in 0.5% Triton X-100 (1X PBS) for 10 min. For FLAG Immuno-FISH, FISH was done before immunostaining. The slides were incubated in 20% glycerol (1X PBS) for 30 min and then freeze-thawed in liquid nitrogen 4 times. The slides were again washed in 0.05% Triton X-100 (3 × 5 min). Depurination was carried out in 0.1 N HCl for 10 min and again washing was done for 3 × 5 min in 0.05% Triton X-100. Equilibration was carried out in 2X SSC for 5 min and then in 50% formamide (2X SSC) over night at room temperature. Slides were denatured in 70% and 50% formamide for 3 min and 1 min, respectively, at 73°C. A total of 10 μl of labeled total human chromosome specific DNA probes (Applied Spectral imaging) was denatured for 7 min at 80°C, re-annealed at 37°C for 20 min and hybridized onto the slides for 2–3 days at 37°C. Post hybridization, washes were done at 73°C in 0.4X SSC (3 × 3 min) and 4X SSC with 0.1% Tween20 (3 × 3 min). Immunostaining for the FLAG tag was done as described earlier in order to identify the H2AX construct expressing cells. The slides were then stained with TO-PRO-3 (Life Technologies) and confocal images with stacks of 0.3 μm optical sections of at least 30 nuclei (in 2 independent experiments), were obtained using a Zeiss confocal laser scanning microscope (LSM510) at 100x magnification. The distance between the nuclear centre and the centre of the chromosome territory (centre here refers to the center of mass) was measured using Bitplane Imaris software.

For NM1 Immuno-FISH, immunostaining was done before FISH. All the steps were same as described above. After immunostaining, the cells were fixed by using 4% PFA for 10 min, washed with PBS and then subjected to all the FISH steps, starting with incubation in 20% glycerol and finally the cells were mounted in Vectashield mounting media containing DAPI.

Two-dimensional Fluorescence *in situ* hybridization (2D-FISH)

2D-FISH was performed using a protocol described earlier (46). Briefly, cells were trypsinized and the pellet was resuspended in hypotonic 0.075 M KCl solution. This was followed by their fixation in 3:1(v/v) methanol: acetic acid. Cells were dropped on slides and subjected to sequential 70%, 90%, 100% ethanol treatment. Denaturation was performed at 70°C for 2 min in 70% formamide (2X SSC). Ten microliters of labeled human chromosome DNA probe (Applied Spectral Imaging) that had been denatured at 80°C for 7 min and re-annealed at 37°C for 20 min, was applied to the denatured cells. Hybridization was done at 37°C overnight. Post hybridization, washes were performed at 72°C in 0.4X SSC (3 × 3 min) and 4X SSC with 0.1% Tween20 (3 × 3 min). Cells were mounted in Vectashield containing DAPI. At least 100 nuclei were imaged on a Zeiss Axiovert 200 microscope at 100x magnification and processed through the software package IMACULAT (76,77) for quantitation of the probe signal. One-way ANOVA and t-tests were performed.

Nuclear fractionation and Western blotting

A previously described nuclear fractionation protocol was used (78). Cells (1×10^6) were resuspended in buffer A [10 mM HEPES (pH = 7.9), 1.5 mM $MgCl_2$, 10 mM KCl, 1 mM DTT, 1X protease inhibitor cocktail (Roche)] and were incubated on ice for 5 min. Nuclei were collected in the pellet fraction by centrifuging at 1300 g, 4 min, 4°C. The nuclei were washed once with buffer A, followed by the addition of buffer B [3 mM EDTA, 0.2 mM EGTA, 1 mM DTT, 1X protease inhibitor cocktail] for 10 min to lyse the nuclei. Centrifugation at 1700 g, 4 min, 4°C was used to collect the insoluble chromatin fraction in the pellet and the nuclear soluble fraction (NS) in the supernatant. The pellet was washed once with buffer B and centrifuged again. The final chromatin enriched pellet (CP) was dissolved in Laemmli buffer and sonicated thrice (15 s pulse) using a Branson sonicator.

For salt extraction, chromatin pellets from cells were incubated in 200, 400 and 800 mM NaCl containing buffer B, kept on ice for 30 min and centrifuged at 20 000 g for 10 min. Equal volumes of supernatant (soluble fraction) and pellet were loaded on the gel for subsequent Western blotting.

For whole cell lysates, cells were washed with 1X PBS twice. The pellet was resuspended in 1X RIPA buffer containing protease inhibitor cocktail (Roche) and incubated on ice for 30 min. The lysate was centrifuged at 14 000 r. p. m. for 10 min at 4°C.

Protein concentrations were determined by using the BCA assay (Pierce BCA kit) and 30 μg of protein was used for immunoblotting. Western blotting of the nuclear soluble (NS) and the CP fractions was done by separating the proteins on a SDS PAGE gel (8% resolving gel for NM1, INO80, ALDHIAI and 15% resolving gel for H2AX, FLAG, actin) and blotting onto PVDF membrane. The membrane was then probed with antibodies for Nuclear myosin1β [for detecting NM1] (Sigma-Aldrich), actin (Sigma-Aldrich), α-Tubulin (Sigma-Aldrich), FLAG (Sigma-Aldrich), INO80 (Abcam), ALDHIAI (Abcam), Rad51 (Santa Cruz Biotechnology), H2AX (Abcam), GSK3β (Cell Signaling) or PhosphoSer9GSK3β (Cell Signaling) as mentioned in the figure legends. NM1, INO80 or actin levels in the nuclear fractions were quantified using ImageJ software, by normalizing the Western blot band intensity with the total coomassie protein load intensity (after subtracting the equivalent background of the blank) for the fraction and plotted as fold change. Total coomassie protein load was used as a loading control (79–81) instead of conventional loading controls such as actin, tubulin because we observed changes in actin (Supplementary Figure S4: Panel E) and tubulin levels in the nuclear fractions upon DNA damage. Because of this observed variability, we could not use these markers as reliable loading controls. Histones also could not be used as a loading control in the Western blots for the nuclear fractionation experiments as they showed up in only the chromatin pellet fraction and not in the nuclear soluble fraction. For whole cell lysates, α-tubulin was used as a loading control.

RESULTS AND DISCUSSION

Blocking ϒ-H2AX signaling leads to inhibition of DNA damage dependent chromosome territory relocation

Certain gene rich chromosomes have been shown to relocate upon induction of DNA damage (46). However, how DNA damage signals such a response is not very clear. In order to understand the same, we decided to assess the role of ϒ-H2AX – an early chromatin modification at DSBs. ϒ-H2AX signaling was down regulated using a nonphosphorylatable mutant of H2AX. FLAG tagged H2AX wild type or mutant H2AX S139A was transfected into normal human dermal fibroblasts (NHDFs) and the cells expressing these constructs in the pool of transfected cells (∼40–50% of the total selected population) were identified by immunostaining for the FLAG tag.

As expected, the overexpressed FLAG tagged H2AX proteins were incorporated into the chromatin fraction (∼50% of the total H2AX) of the nuclei as observed by immunoblotting of the FLAG tag in the CP (Supplementary Figure S1: Panel A and B). To ensure that following cisplatin damage cells expressing the H2AX constructs are not undergoing cell death, cells showing apoptotic changes such as nuclear fragmentation, membrane blebbing and DNA condensation were quantified (82,83). Since the percentage of apoptotic nuclei in the H2AX wild type and H2AX S139A expressing cells in the absence or presence of cisplatin damage (25 μM for 4 h) was found to be under 12% (Supplementary Figure S1: Panel C), subsequent studies on CT positions in these cells following DNA damage were carried out using the same regime.

Cells expressing the mutant H2AX S139A showed fewer number of ϒ-H2AX foci upon cisplatin damage than those in either untransfected or H2AX wild type transfected control cells (Figure 1A–C). Since only half of H2AX in the chromatin comprises of mutant form of protein (Supplementary Figure S1: Panel B), therefore we surmise that the same must have acted as dominant-negative in order to show a decrease in the overall ϒ-H2AX foci count. It was also assessed whether such decrease in ϒ-H2AX levels in the mutant cells leads to a concomitant drop in its downstream protein signaling targets. After DNA damage, levels of 53BP1 levels have been observed to increase (84–86), following which ϒ-H2AX signaling leads to the accumulation of 53BP1 at DSB sites (18,86). It has been suggested that the role of phosphorylated 53BP1 can be uncoupled from DSB repair, as the binding of 53BP1 to DSBs has been found to be independent of its phosphorylation status (87). We therefore monitored total 53BP1 levels in H2AX S139A cells and compared the same with untransfected and H2AX wild type transfected cells following DNA damage. Similar to earlier reports in normal human fibroblasts (85,88), we also observed that untransfected, H2AX wild type or H2AX S139A mutant expressing NHDFs without any damage exhibited faint immunostaining of 53BP1. Moreover, as expected, nearly all the nuclei (∼100%) in the case of untransfected NHDFs or H2AX wild type expressing control cells showed high levels (mean intensity > 27 a.u.) of total 53BP1 following cisplatin damage. In contrast, only 21.8% of H2AX S139A expressing cells displayed high levels of
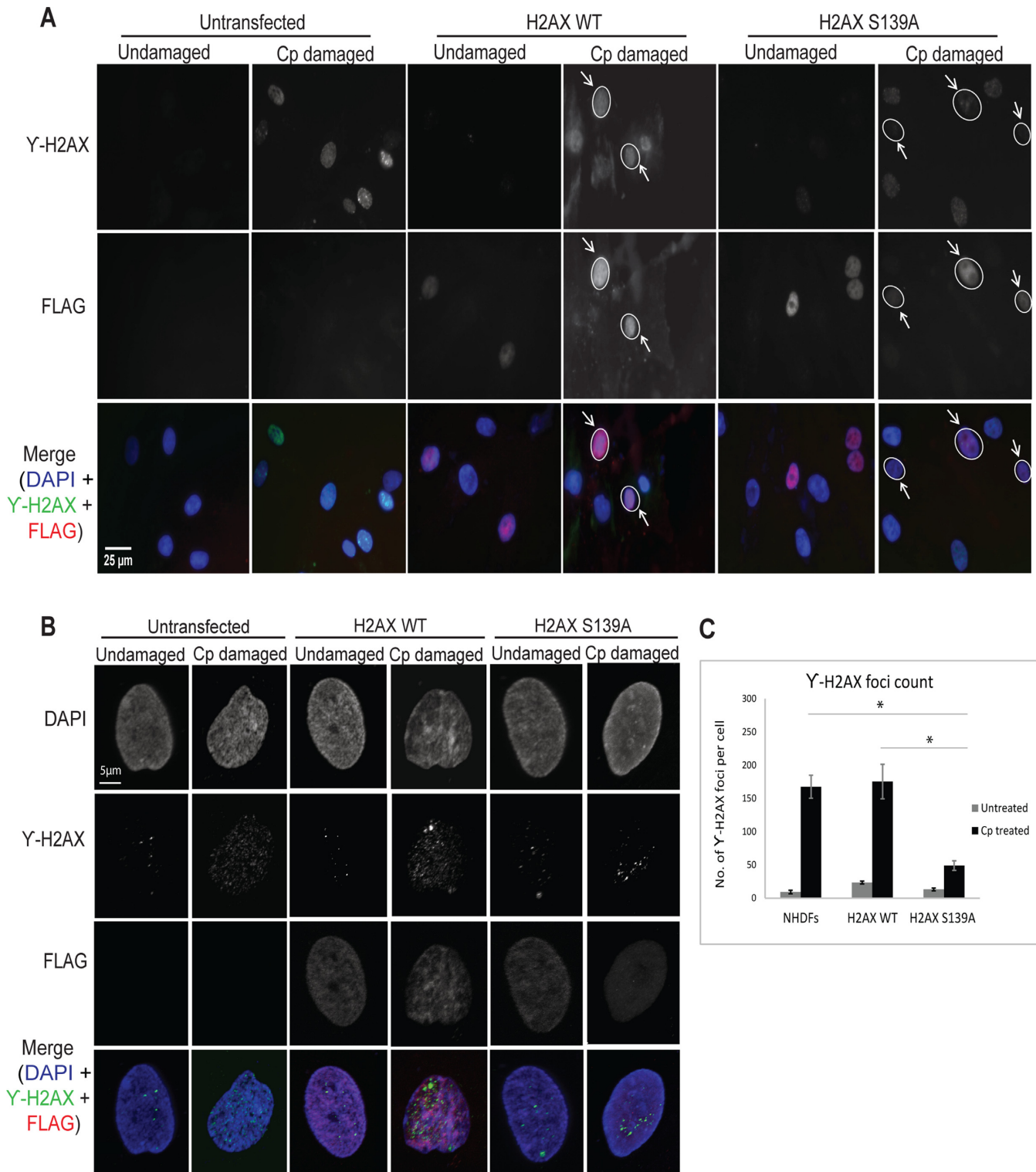
Figure 1. ϒ-H2AX foci are reduced in H2AX S139A transfected cells. H2AX transfected NHDFs were identified by staining for FLAG (red). ϒ-H2AX staining (green) was visualized in untransfected, H2AX wild type and H2AX S139A transfected NHDFs under undamaged or Cp (cisplatin) damaged conditions. (**A**) Images were taken at 40x magnification in order to show the effect of H2AX S139A mutant construct in a population of cells. Arrows point to FLAG positive nuclei in Cp treated H2AX wild type or S139A transfected cells. (**B** and **C**) Quantitation of ϒ-H2AX foci in untransfected, H2AX wild type and H2AX S139A expressing cells was performed on confocal images taken at 100x magnification using Imaris software. N = 2, n = 25. Error bars represent the s.e.m. * indicates $P < 0.05$.

53BP1 (Figure 2A and B) and the remaining large fraction of nuclei in these cells showed only basal levels of 53BP1 even after DNA damage. Recruitment of chromatin remodeler INO80 has been shown to ensue via direct interaction with ϒ-H2AX foci at the DSB sites (17). Therefore, we assessed the protein levels of the INO80 in the nuclear soluble and chromatin fractions in H2AX S139A cells before and after cisplatin damage. In nuclear fractionation experiments, the total coomassie protein load was used as a loading control (79–81) instead of conventional loading controls such as actin, tubulin because we observed changes in actin (Supplementary Figure S4: Panel E) and tubulin levels in the nuclear fractions upon DNA damage. The recruitment of INO80 to the chromatin pellet fraction did not increase in mutant cells upon DNA damage, which contrasted from that of untransfected or wild type H2AX expressing cells where INO80 levels were increased in the chromatin fraction following damage (Figure 2C–F). All these results put together confirmed that the decrease in ϒ-H2AX foci number led to a concomitant reduction of its downstream signaling in the mutant H2AX expressing cells following DNA damage.

In order to understand the role of ϒ-H2AX in DNA damage induced CT relocations, the positions of chromosomes 19, 15 and 11 were monitored in cells expressing mutant ϒ-H2AX and compared with their control counterparts. Positions of these chromosomes were not significantly changed in the untransfected and H2AX transfected cells (Supplementary Figure S2: Panel D) in the absence of any DNA damage. Upon DNA damage, in control cells the relocation of chromosome 19 from nuclear interior to nuclear periphery and chromosome 15 from nuclear periphery to the interior was observed and this corroborated our earlier results (46) (Figure 3A and B). However, such DNA damage induced relocation of both these chromosomes was not observed in the cells expressing mutant H2AX S139A construct (Figure 3C). Chromosome 11 whose position (peripheral to intermediate within the nucleus) remains unaltered following DNA damage (46) was taken as a negative control and as expected its position remained unchanged in the untransfected cells as well as the H2AX construct expressing cells following DNA damage. Volumes of the CTs were not significantly altered in undamaged *versus* cisplatin damaged conditions in the control cells (untransfected, H2AX wild type transfected) and H2AX S139A transfected cells (Supplementary Figure S3: Panel A–C).

Since cisplatin damage induced CT relocation fails to occur in H2AX S139A mutant expressing cells, this indicates that ϒ-H2AX signaling is required for the CT relocation during DDR. ϒ-H2AX recruits chromatin remodelers such as INO80 and NuA4 near the DSB sites, thus rendering them more accessible to the repair machinery (16–18,89). Therefore, it can be speculated that by remodeling chromatin at multiple DSB sites, ϒ-H2AX signaling may lead to a concerted structural change at a whole chromosomal level, finally guiding DNA damage induced CT relocation.

Inhibition of late steps of repair catalyzed by Rad51 or DNA ligase IV do not fully abrogate damage dependent CT relocation

Earlier we had reported that initial sensing and repair of the DSBs by ATM kinase and DNAPK play an important role in damage induced relocation of CTs (46). In order to assess what happens to CT relocation when later stages of DSB repair are inhibited, we analyzed cells in which the function of DNA ligase IV or Rad51 [repair proteins that function during relatively later stages of NHEJ and HR pathways, respectively (90–93)] is inhibited or knocked down. The technique of 2D-FISH was used for the analysis of CT positions in these experiments. 2D-FISH is a relatively more facile technique in comparison to 3D-FISH and when statistically high number of nuclei (at least 100 per experiment) are analyzed, 2D-FISH does indeed corroborate the CT positions uncovered by 3D-FISH (40,46,77).

Inhibition of DNA ligase IV by a specific chemical inhibitor SCR7 (94–96), resulted in partial relocation of CT 19 and near complete relocation of CT 15 following 4 h of cisplatin damage (Figure 4A). A similar result was observed in the case of Rad51 siRNA treated cells in comparison to the control siRNA treated cells (Figure 4B). It is plausible that CT 19 being most gene dense chromosome is more sensitive to inhibition of late repair steps (NHEJ or HR), leading to some effect on its CT dynamics. But clearly CT 15 dynamics were relatively unaffected by inhibition in these late repair steps. Expectedly, position of the negative control CT 11 (peripheral to intermediate) remained unchanged post cisplatin damage under all these conditions. Since cisplatin damage treatment exceeding 6–7 h resulted in significantly higher level of cell death in DNA ligase IV inhibitor treated and Rad51 knockdown conditions, CT positioning analyses at longer time points of damage treatment were not carried out. The partial (CT 19) or nearly complete (CT 15) relocation of CTs in response to DNA damage, when the function of late repair proteins DNA ligase IV or Rad51 are inhibited/knocked down suggests that the early steps of DSB repair play a more important role in CT relocation than the later stages of repair. In fact such partial effects on CT repositioning might be an indirect consequence of repair inhibition impacting the early sensors and effectors. Initiation of damage sensing and signaling that does not accomplish DNA repair (due to inhibition of late players of repair) may feedback inhibit ongoing CT relocation leading to partial inhibitory effects.

Nuclear myosin 1 (NM1) recruitment to chromatin is enhanced by DNA damage treatment

DNA damage induced CT relocation is specific to certain gene rich chromosomes and therefore, does not seem to be a random diffusion based process. The motor protein NM1 has been implicated in whole chromosome repositioning during serum starvation (40) and also in the repositioning of a chromosomal domain (58). To assess if the same motor protein is involved in the context of DNA damage induced CT repositioning, the levels of this protein were analyzed before and after DNA damage. NM1 levels in the chromatin fraction were already high in control NHDFs even in the absence of DNA damage (Figure 5A). Such
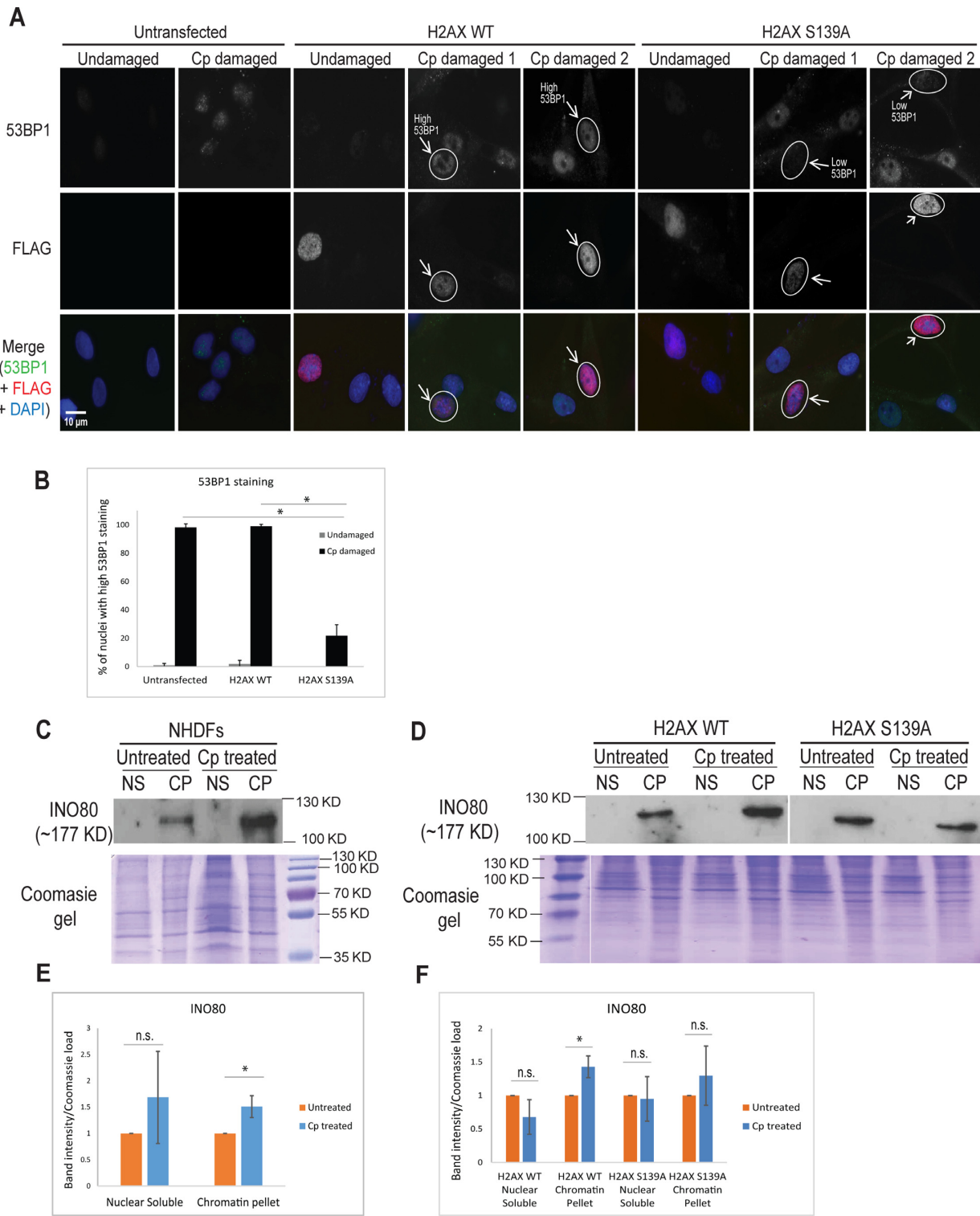
Figure 2. ϒ-H2AX signaling is reduced in H2AX S139A transfected cells. (**A**) Total 53BP1 staining in untransfected, H2AX wild type and H2AX S139A transfected NHDFs under undamaged or Cp (cisplatin) damaged conditions. Images were taken at 63x magnification. Arrows point to FLAG positive nuclei in the FLAG-H2AX transfected population. (**B**) Quantification of nuclei that showed high levels (Mean intensity > 27 a.u.) of total 53BP1 following damage. N = 2, n = 55. (**C**) Representative images of INO80 Western blots in untransfected, (**D**) H2AX WT and H2AX S139A transfected NHDFs in the absence or presence of cisplatin treatment. NS = Nuclear soluble, CP = Chromatin pellet. Lanes in the blot have been spliced together in the sample order same as that of the coomassie gel loading control in (**D**). N = 3 for Western blots. (**E**) Quantitation of INO80 levels in nuclear fractions of untransfected, (**F**) H2AX WT and H2AX S139A transfected NHDFs in the absence or presence of cisplatin treatment. INO80 levels in the nuclear fractions were quantified using ImageJ software, by normalizing the Western blot band intensity with total coomassie protein load intensity (loading control) for the fraction and plotted as fold change. NS = Nuclear soluble, CP = Chromatin pellet. N = 3. *P*-values calculated using Student's *t*-test. Error bars represent the s.d., * indicates $P < 0.05$, n.s. = not significant.
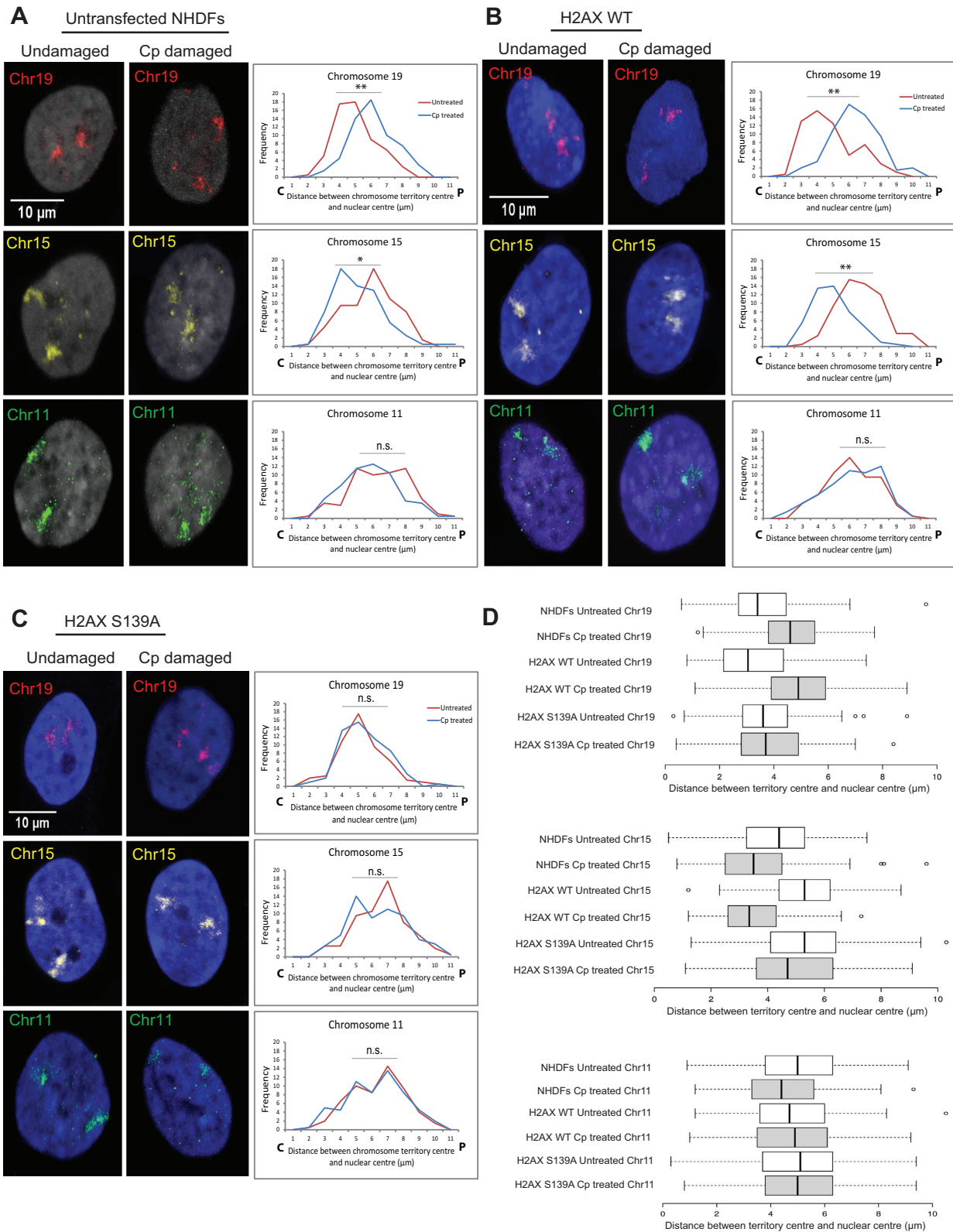
Figure 3. Chromosome territory repositioning requires ϒ-H2AX signaling. Immuno-FISH was performed, where H2AX wild type and S139A expressing cells were identified by FLAG (blue) immunostaining, followed by FISH for chromosome 19 (red), 15 (yellow) and 11 (green). Nuclei were visualized by TO-PRO-3 staining (grey). Territory position is expressed as a frequency distribution of either (**A**) untransfected or (**B** and **C**) FLAG positive transfected nuclei. Distance (in μm) between the nuclear centre and CT centre in 3D confocal images (63x magnification) was quantitated using Imaris software. N = 2, n = at least 30 nuclei. *P*-values were calculated using Kolmogorov–Smirnov test. * and ** indicate *P* < 0.05 and *P* < 0.01 respectively. n. s. = not significant. (**D**) Box plots generated using the web tool BoxPlotR (113) for the same data are displayed. The box plots span the second quartile, median and the fourth quartile of the distances, while negative and positive error bars represent the minimum and maximum distances. On box plot Y-axis Cp = Cisplatin damaged. On frequency distribution graphs C = Centre of nucleus, P = Periphery of nucleus.
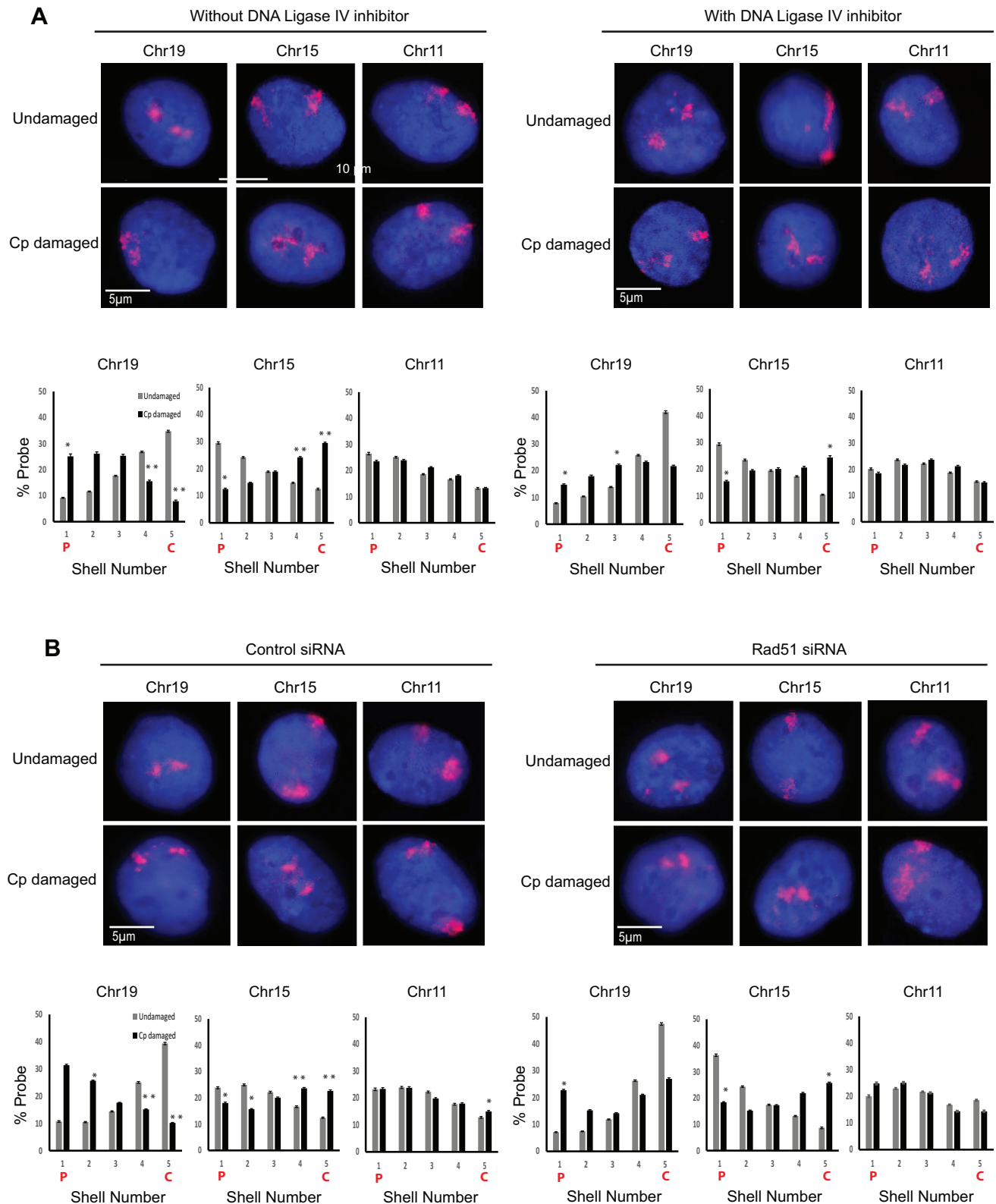
Figure 4. Partial or no effect on CT relocation upon inhibition of DNA ligase IV or Rad51 function. Positions of chromosomes 19, 15 and 11 were assessed by 2D-FISH in (**A**) cells treated with or without DNA ligase IV inhibitor; (**B**) control siRNA and Rad51 siRNA treated cells. 2D-FISH images were analyzed and quantitated by using the computational script IMACULAT (76,77). X-axes of the graphs depict the nuclear shell number, with 1 being as the outermost and 5 being the innermost shell. Y-axes of the graphs show the percentage of probe normalized to DAPI. N = 2, n > 100 nuclei. Error bars represent the s.e.m. *P*-values calculated using Student's *t*-test.* and ** indicate *P* < 0.05 and *P* < 0.01, respectively; n.s. = not significant. On graphs C = Centre of nucleus, P = Periphery of nucleus.
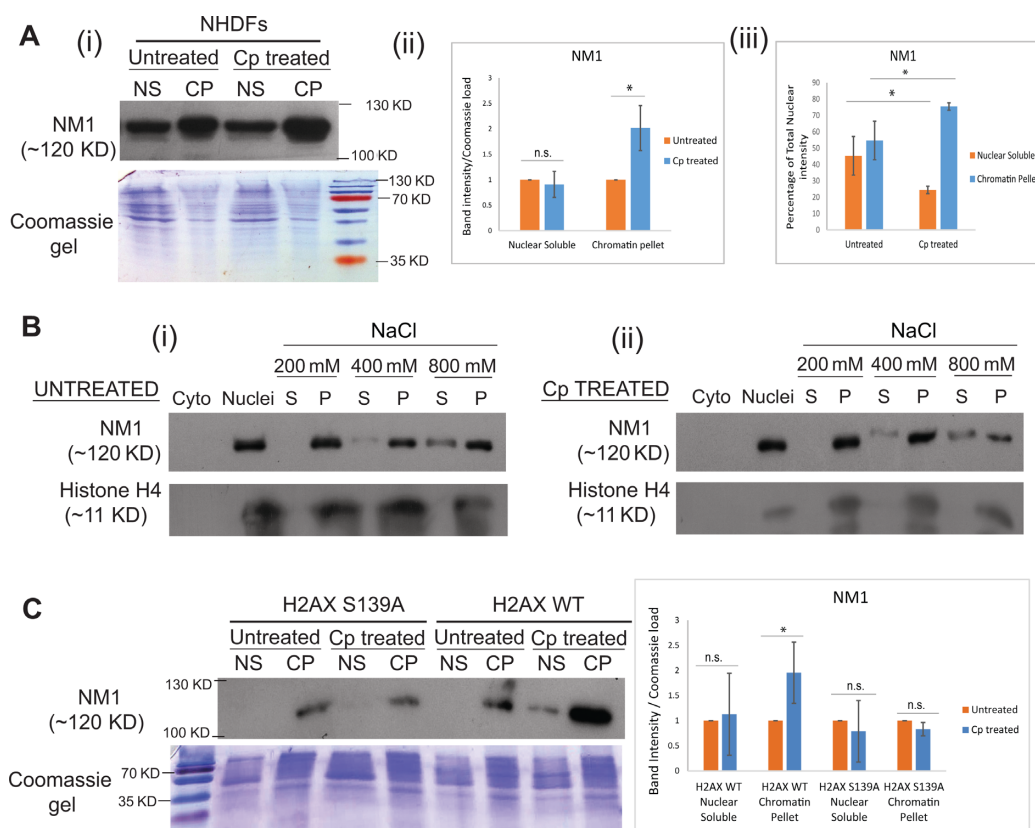
Figure 5. Nuclear myosin 1 level increases in chromatin fraction upon DNA damage which depends on Υ-H2AX function. (**A**) Levels of NM1 in nuclear fractions of untransfected NHDFs were assessed by Western blotting before and after cisplatin damage and plotted as (i) fold change or (ii) percentage of total NM1 intensity. N = 3. (**B**) Salt extraction of NM1 from insoluble chromatin pellet fraction with increasing concentrations of NaCl. Histone H4 was taken as a control. S = Soluble fraction, P = Pellet fraction. N = 2 (**C**) Representative Western blot for H2AX wild type and H2AX S139A expressing cells under undamaged and cisplatin treated conditions. N = 3. The image is an under exposure to prevent oversaturation of the signal in the Cp treated H2AX wild type chromatin pellet fraction lane. NS = Nuclear soluble, CP = Chromatin pellet. NM1 levels in the nuclear fractions were quantified using ImageJ software, by normalizing the Western blot band intensity with total coomassie protein load intensity (loading control) for the fraction and plotted as fold change or percentage of total NM1 in the nucleus. *P*-values calculated using Student's *t*-test. Error bars represent the s.d., * indicates *P* < 0.05 and n.s. = not significant.

high levels of chromatin bound NM1 are consistent with its functional roles in nuclear processes such as transcription and chromatin remodeling, etc. (64–66,68,97). Interestingly upon cisplatin damage, the levels of NM1 in chromatin fraction showed a measurable increase (~1.5- to 2-fold) as compared to undamaged control (Figure 5A (ii)). However, surprisingly the levels of NM1 in the whole cell lysates (Supplementary Figure S4: Panel B) or whole nuclei (Supplementary Figure S4: Panel C) did not seem to change after cisplatin damage. The relative levels of NM1 in undamaged cells (the nuclear soluble (NS) versus chromatin pellet (CP) fraction with respect to the total nuclear NM1 after normalization for differential protein load) showed ~55% of NM1 in the CP fraction, while the remaining was in NS form. Following cisplatin damage, the chromatin bound NM1 increased to ~76% of the total nuclear NM1 (Figure 5A (iii)). These results were also corroborated by immunostaining experiments, where high number of NM1 puncta within the nucleus were observed even in undamaged state, with an increase in the number of puncta following DNA damage (Supplementary Figure S6: Panel A and B). Marginal increase in NM1 puncta following DNA damage is consistent with ~1.5- to 2-fold increase in chromatin bound

NM1 observed in the Western analysis. Such an increase in chromatin bound NM1 occurred after at least two types of DNA damages, as cells treated with hydrogen peroxide also showed similar (~1.5-fold) increase in the chromatin bound protein (Supplementary Figure S4: Panel D).

To assess the strength of interactions of NM1 with chromatin, salt extraction of NM1 from the chromatin pellet was done with increasing concentrations of NaCl (Figure 5B). NM1 started dissociating from the chromatin pellet into the soluble fraction at 400 mM NaCl, but most of the protein was still associated with the pellet fraction of chromatin even at 800 mM NaCl concentration. Histone H4, a tightly bound protein in the chromatin, was taken as an internal control and as expected it did not elute into the soluble fraction even at 800 mM NaCl. These data indicated that NM1 is a stably bound component of chromatin fraction, but starts eluting at a NaCl concentration lower than that required for a core histone such as H4. Cisplatin damaged nuclei exhibited an essentially similar elution profile of NM1 and H4 proteins as the undamaged control nuclei. Interestingly, the nature of association of NM1 with chromatin does not seem to get affected following DNA damage.

However, uncovering the details of the same need further experimental probing.

Surprisingly, in untransfected NHDFs the levels of actin in both the nuclear soluble and the chromatin fraction decreased upon cisplatin induced DNA damage (Supplementary Figure S4: Panel E). It has been reported that nuclear actin and myosin have uncoupled roles in the nuclear functions (67,68). Therefore, the damage induced increase in chromatin bound NM1 and the decrease in actin levels in the nucleus that we have observed may reflect a differential regulation of activities of the two motor proteins in the nucleus. How DNA damage signaling regulates the activity of these proteins differentially during DDR remains to be investigated.

DNA damage dependent increase of NM1 recruitment to chromatin is mediated by ϒ-H2AX signaling and requires DNA damage sensors

In the previous experiment, we showed that induction of DNA damage leads to enhanced recruitment of NM1 to chromatin. In order to test if ϒ-H2AX signaling has any role in the recruitment of NM1 to the chromatin as well as the repositioning of CTs following DNA damage, we analyzed the levels of NM1 in the chromatin fraction in ϒ-H2AX wild type and compared it with that in H2AX S139A mutant expressing cells. The wild type H2AX construct expressing cells showed the expected increase in NM1 recruitment to the chromatin fraction just like the untransfected NHDFs. Surprisingly, such an increase in chromatin bound NM1 was not observed in H2AX S139A expressing cells and the recruitment of NM1 to the chromatin fraction remained unchanged in these cells before and after cisplatin damage (Figure 5C). Therefore, these results suggest that ϒ-H2AX signaling is functionally coupled with the cisplatin damage induced enhanced chromatin recruitment of NM1. In our previous study (46), we had shown that the recognition of DNA damage by sensor and repair proteins, such as ATM kinase and DNAPK precedes CT relocation. Therefore, we tested if such DNA damage induced recruitment of NM1 to the chromatin fraction also requires the function of DSB sensors such as ATM, ATR kinase, PARP-1 and DNAPK. As reported earlier (98–100), ϒ-H2AX immunostaining was found to decrease in cells pretreated with ATM, ATR or DNAPK inhibitor following cisplatin damage (Supplementary Figure S5: Panel A–C). Interestingly, we observed that cells upon prior treatment with inhibitors for not only sensor proteins ATM, ATR and DNAPK, but also PARP-1 failed to exhibit enhanced chromatin recruitment of NM1 following cisplatin damage (Figure 6A–D), thereby suggesting that general sensing of DNA damage seems to be mechanistically coupled to the process of NM1 recruitment to the chromatin following DNA damage.

NM1 is essential for chromosome territory repositioning following DNA damage

NM1 is the predominant nuclear isoform encoded by MYO1C gene (59). In order to check if this nuclear motor is essential for CT relocation during DDR, we employed siRNA mediated knockdown of the MYO1C gene (Supple-

mentary Figure S7: Panel A–C). The siRNA knockdown resulted in ∼60–70% reduction in NM1 levels as assessed by Western analysis. By using chromosome-specific 2D-FISH analysis (46,76,77), we assessed the positions of chromosome 19, 15 and 11 in cells transfected with control and MYO1C siRNA. Such analyses corroborated our results that control NHDFs (treated with the control siRNA) exhibited the expected relocation of chromosome 19 from the nuclear interior to the periphery upon cisplatin damage and *vice versa* for chromosome 15. However, in the same experimental conditions, MYO1C knockdown cells failed to show any damage induced relocation of chromosome 19 and 15 (Figure 7). Expectedly, chromosome 11 taken as a negative control did not show any spatial relocation following DNA damage in cells treated with either siRNA. Since, the MYO1C siRNA that has been used for RNAi experiment (Figure 7) is a mixture of oligonucleotide probes directed against entire MYO1C gene and thus siRNA effects may not be specific to any particular isoform of myosin 1C, as any of or all three isoforms (a, b or c – all of which are found in the nucleus) might have been down regulated in the siRNA experiment. Since NM1 levels certainly decrease following the siRNA treatment as observed by Western blotting and IF analyses (Supplementary Figure S7: Panel A–C), it is clear that NM1 is definitely required for the process of CT relocation during DDR. The specific participation of the myosin 1C isoforms, if any, in CT relocation remains to be investigated and it would be interesting to uncover if these three nuclear isoforms cross-talk/coordinate with each other in the context of DNA damage and repair.

NM1 mutants that have impaired motor function are unable to associate with RNA polymerase I and rDNA (66,69). To understand how the motor activity of NM1 influences its enhanced chromatin binding and CT relocation post DNA damage, cells over-expressing V5 tagged NM1 motor function defective mutant (G126S- that has defective ATPase function) or wild type NM1 were analyzed (66). As expected, in the control cells expressing wild type NM1, damage induced increase in chromatin recruitment of NM1 and CT relocation were observed (Figure 8). In contrast, the NM1-G126S mutant expressing cells failed to show such DNA damage induced changes (Figure 8), indicating that the motor function of NM1 was important for its binding to chromatin following damage and for the subsequent CT relocation. This is a significant mechanistic insight highlighting the importance of nuclear myosin's motor function not only for its association with Pol I transcriptional machinery (66) but also for its binding to chromatin following DNA damage and mediating CT repositioning. It is important to note here that the resident level of NM1-G126S in chromatin fraction prior to DNA damage does not seem to change compared to wild type NM1 (Figure 8A). Moreover, a previous study has shown that an impaired motor activity mutant of NM1 protein (RK605AA) fails to recruit to rDNA chromatin; we believe that our bulk chromatin fractionation assay does not seem to capture such finer details of NM1 recruitment (69). However, the results of experiments involving dominant negative G126S mutant of NM1 (Figure 8) do seem to reinforce the result of siRNA experiment (Figure 7) that isoform NM1 certainly does participate in the CT relocation occurring post cisplatin damage.
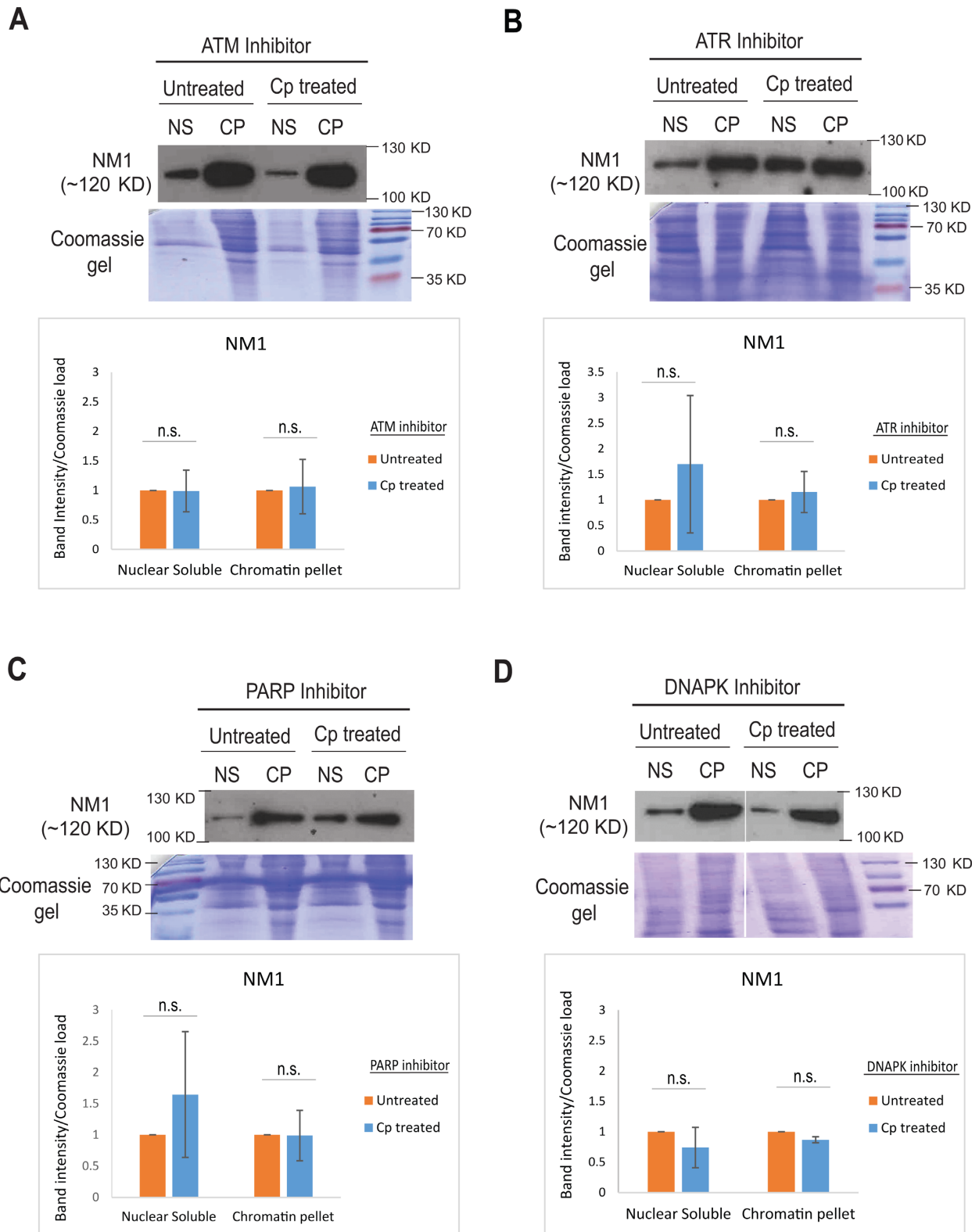
Figure 6. Increased nuclear myosin 1 recruitment to chromatin requires DNA damage sensors. Representative Western blots for NM1 in cells subjected to treatment with inhibitors of (**A**) ATM, (**B**) ATR, (**C**) PARP-1 and (**D**) DNAPK before cisplatin damage and the quantitation of the blots. NS = Nuclear soluble, CP = Chromatin pellet. NM1 levels in the nuclear fractions were quantified using ImageJ software, by normalizing the Western blot band intensity with total coomassie protein load intensity (loading control) for the fraction and plotted as fold change. N = 3. Lanes from the same blot and gel have been merged together in (D). *P*-values calculated using Student's *t*-test. Error bars represent the s.d., * indicates $P < 0.05$ and n.s. = not significant.
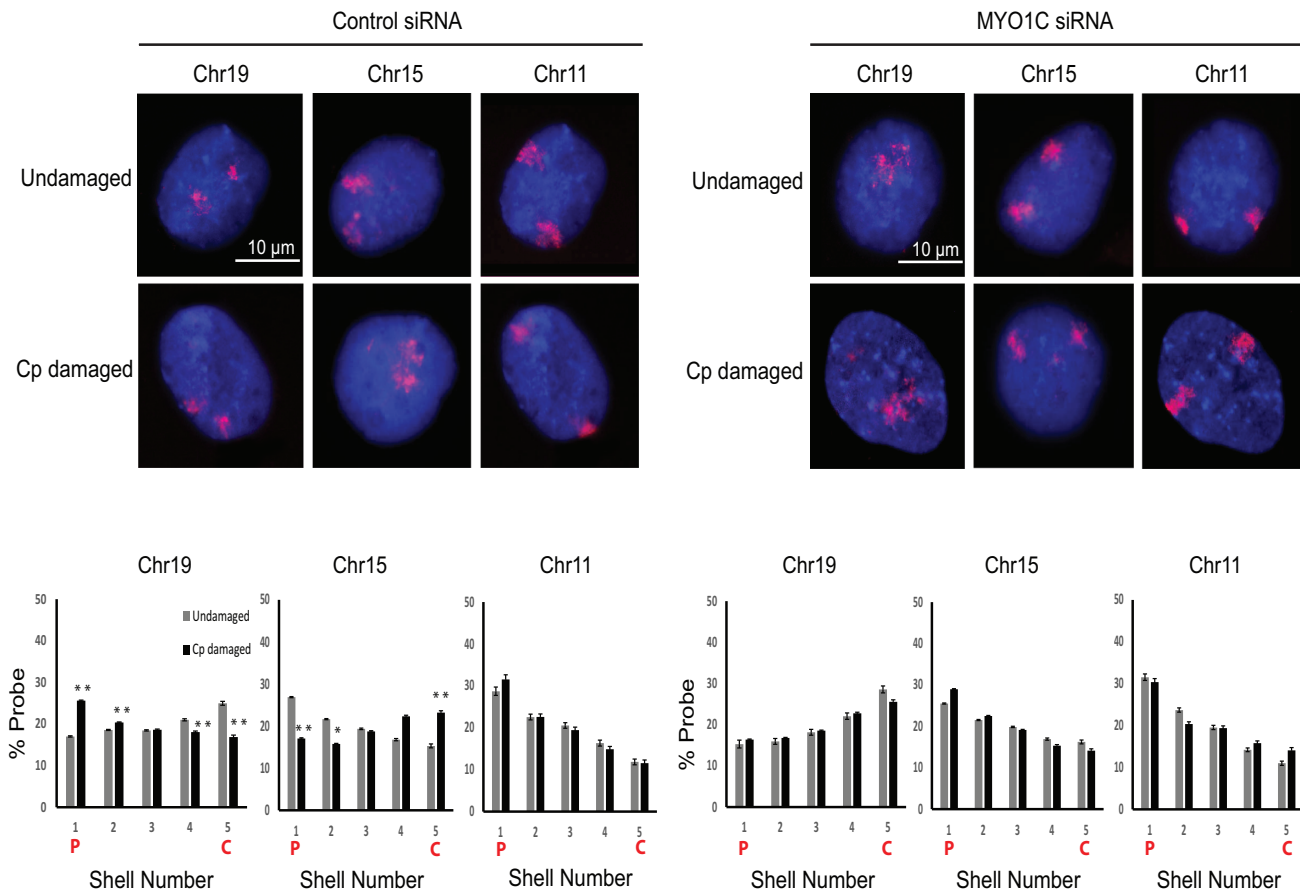
Figure 7. Nuclear myosin 1 (NM1) is required for the relocation of chromosome territories. Positions of chromosomes 19, 15 and 11 were assessed by 2D-FISH in control siRNA and MYO1C siRNA treated cells. 2D-FISH images were analyzed and quantitated by using the computational script IMACULAT (76,77). X-axes of the graphs depict the nuclear shell number, with 1 being as the outermost and 5 being the innermost shell. Y-axes of the graphs show the percentage of probe normalized to DAPI. N = 2, n > 100 nuclei. Error bars represent the s.e.m. *P*-values calculated using Student's *t*-test. * and ** indicate $P < 0.05$ and $P < 0.01$, respectively; n.s. = not significant. On graphs C = Centre of nucleus, P = Periphery of nucleus.

The phosphorylation of NM1 by GSK3β kinase has been reported to regulate NM1 binding to rDNA (73). In order to test if such phosphorylation of NM1 is also required for the increased chromatin binding of NM1 and subsequent CT relocation following DNA damage, we inhibited GSK3β kinase using LiCl, a commonly used specific inhibitor of this kinase (101–107). We confirmed the inhibition of GSK3β, by monitoring its inactive form Phospho-Ser-9 GSK3β (103,104,107). In cells treated with LiCl, the inactive phospho-form of GSK3β increased in comparison with the untreated cells (Supplementary Figure S9), implying that addition of LiCl inhibited GSK3β in our experimental conditions. Following this, we compared NM1 levels in chromatin fraction as well as CT positions, before and after cisplatin damage. It was observed that the damage induced increase in NM1 recruitment to chromatin and CT relocation occurred in both untreated control as well as LiCl treated cells (Figure 9), suggesting that the phosphorylation of NM1 by GSK3β does not seem to impact DNA damage induced NM1 functions. We also probed for changes in phospho-NM1 using a phospho-serine-threonine specific antibody on immunoprecipitated NM1 from nuclear solu-

ble and chromatin fractions. The bulk phosphorylation status of NM1 (nuclear soluble or chromatin-bound) was not affected by cisplatin damage treatment (data not shown). Although the bulk phosphorylation of nuclear myosin does not seem to change following DNA damage, this aspect needs further detailed analyses of whether phosphorylation at specific sites of NM1, if any, change in contrast to bulk phosphorylation post DNA damage. It is likely that the analysis of NM1 phosphorylation spectrum may uncover interesting differences specific to transcription versus DNA damage induced functional states of NM1 in chromatin.

NM1 immuno-FISH experiments revealed that though the number of NM1 puncta on chromosome 19 (∼19) (Figure 10) which relocates in response to damage, is slightly higher than that on chromosomes 15 and 11 (∼12) (Figure 10), but there is no statistically significant increase in the number of puncta on these chromosomes following cisplatin damage (Figure 10). Interestingly, the NM1 puncta normalized to chromosome size revealed a higher count for CT 19 (∼0.3) in comparison with that of CTs 15 and 11 (∼0.1). Since the number of NM1 puncta per CT was not
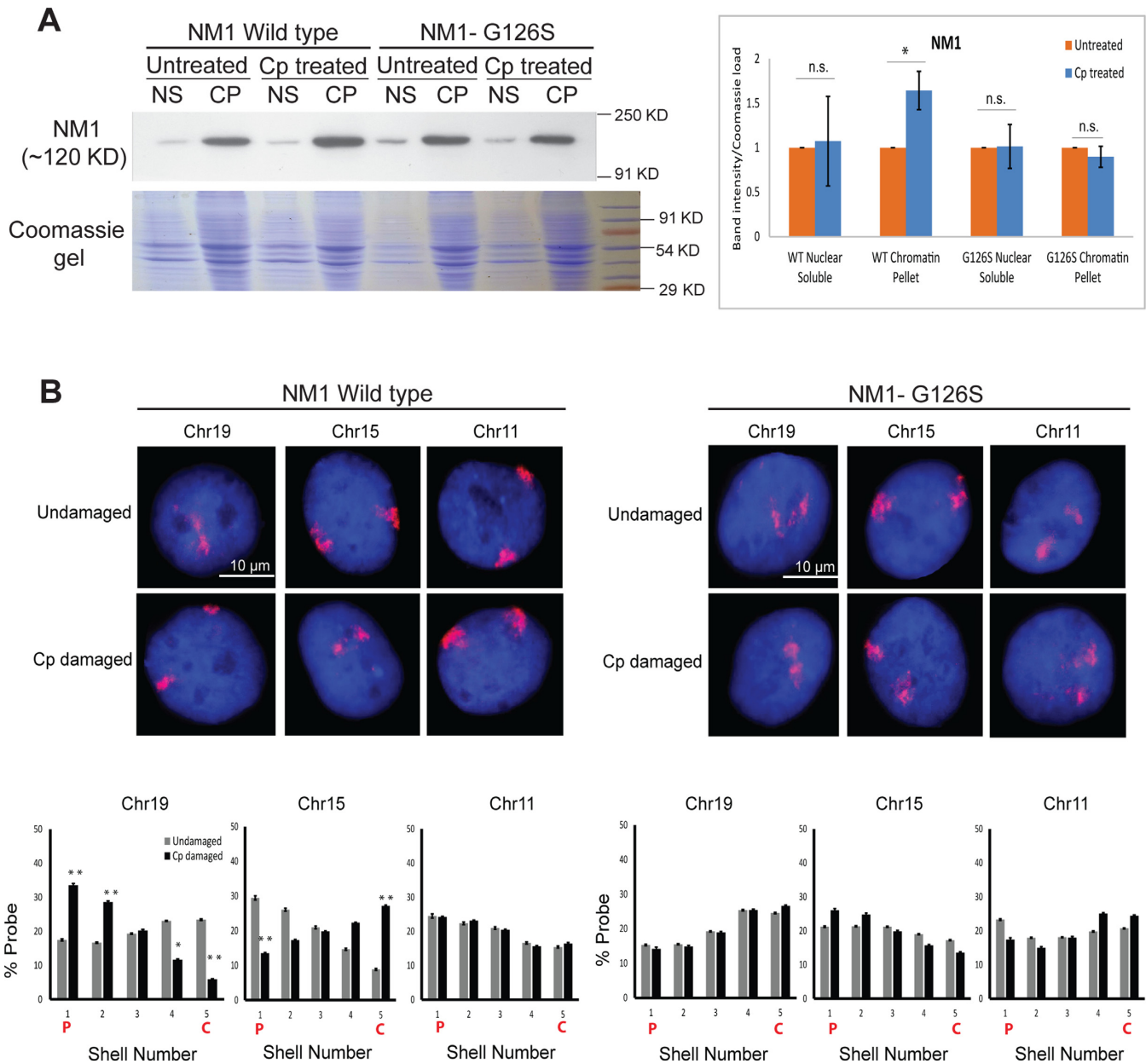
Figure 8. Motor function of NM1 is required for damage induced increase in chromatin binding of myosin and CT relocation. (**A**) Representative Western blots for NM1 in cells overexpressing V5 tagged NM1 wild type or motor mutant G16S. NS = Nuclear soluble, CP = Chromatin pellet. N = 3. *P*-values calculated using Student's *t*-test. Error bars represent the s.d. (**B**) 2D-FISH was used to analyze the positions of CTs 19, 15 and 11 in the NM1 wild type or motor defective over-expressing cells. X-axes of the graphs depict the nuclear shell number, with 1 being the outermost and 5 being the innermost shell. Y-axes of the graphs show the percentage of probe normalized to DAPI. N = 2, n = at least 100 nuclei. On graphs C = Centre of nucleus, P = Periphery of nucleus. Error bars represent the s.e.m. *P*-values calculated using Student's *t*-test. * and ** indicate *P* < 0.05 and *P* < 0.01 respectively; n.s. = not significant.

significantly different following DNA damage, it was not possible to address if the increased pan-chromatin NM1 recruitment (∼1.5- to 2-fold) that we observed earlier following DNA damage could be mapped to specific chromosomes by immuno-FISH analyses. We believe that capturing of contours of CTs by immuno-FISH is not accurate enough to map the myosin puncta to specific territories. Therefore, we cannot address nuclear myosin puncta increase *vis-à-vis* specific CTs with the current resolution of images. Much improved resolution and analyses of CT-conformations/contours is required to address this issue.

Alternately, in order to comprehensively analyze the levels of NM1 on specific chromosomes, one needs to employ a whole-genome based NM1 ChIP Seq method that will be a part of a separate study.

Since we observed that ϒ-H2AX signaling (Figure 3) as well as NM1 recruitment are required for CT relocation, we were prompted to check whether NM1 distribution in the nuclei is in any manner correlated with that of ϒ-H2AX. We observed that while both NM1 and ϒ-H2AX showed DNA damage induced puncta, but these two proteins showed very little, or no spatial co-localization in cisplatin treated cells
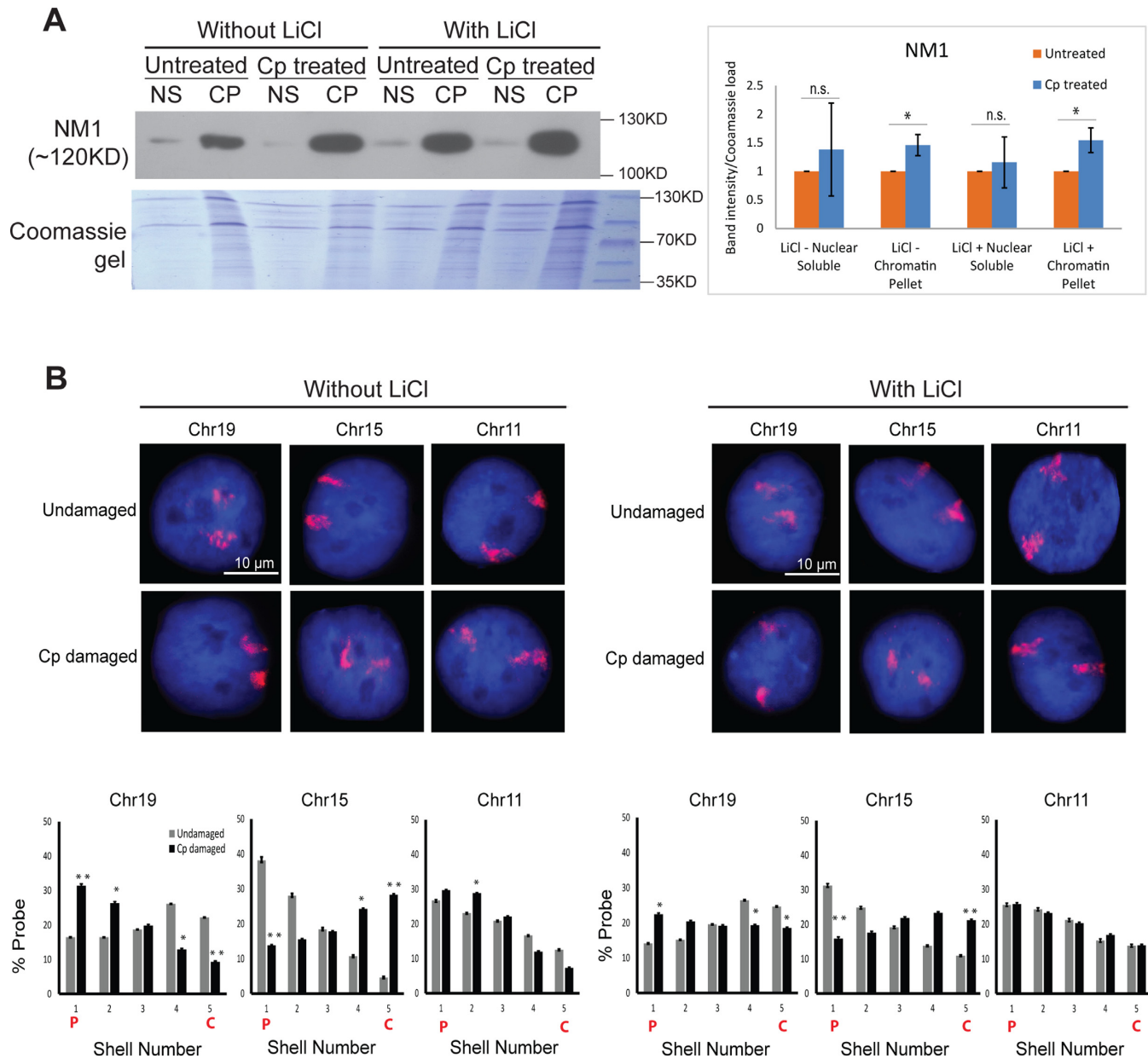
Figure 9. Phosphorylation of NM1 by GSK3β does not seem to be important for damage induced increase in chromatin binding of NM1 and CT relocation. (**A**) Western blotting was used to check the levels of NM1 in cells treated with or without 20mM LiCl (inhibitor of GSK3β kinase) for 3 h. NS = Nuclear soluble, CP = Chromatin pellet. N = 3. Error bars represent the s.d. (**B**) 2D-FISH analysis for CTs 19, 15 and 11 in cells treated with or without 20 mM LiCl. N = 2, n > 100 nuclei. On graphs C = Centre of nucleus, P = Periphery of nucleus. Error bars represent the s.e.m. *P*-values calculated using Student's *t*-test. * and ** indicate $P < 0.05$ and $P < 0.01$ respectively; n.s. = not significant.

(Pearson correlation coeff. < 0.005) (Figure 11). Since NM1 and Υ-H2AX fail to co-localize, the enhanced recruitment of the former to CTs following Υ-H2AX signaling during DDR must be functionally coupled, but perhaps indirectly mediated via some chromatin remodeler, downstream signaling proteins or even nucleoskeletal proteins. The nature of such functional coupling and its eventual culmination into CT relocation changes needs to be probed further.

As described earlier, NM1 is reported to bind to rDNA chromatin as well as Pol II promoters to participate in transcription (69,70,73) and NM1 also mediates chromatin modifications via chromatin remodelers/modifiers such as

WSTF-SNFh2, PCAF and Set1/Ash2 that make chromatin suitable for Pol I or Pol II transcription (64,69,70). It would be interesting to study what happens to such NM1 mediated activating chromatin modifications and NM1 binding to rDNA, Pol II promoters upon DNA damage as global transcription is known to decrease following DNA damage (99,108–111). Moreover, there is also a possibility that some other kind of chromatin remodeling mediated by NM1 following DNA damage could help in the CT remodeling leading to large scale CT relocation during DDR, which is an aspect that also needs further investigation. Moreover the mechanistic role of NM1 in the context of nuclear actin dur-
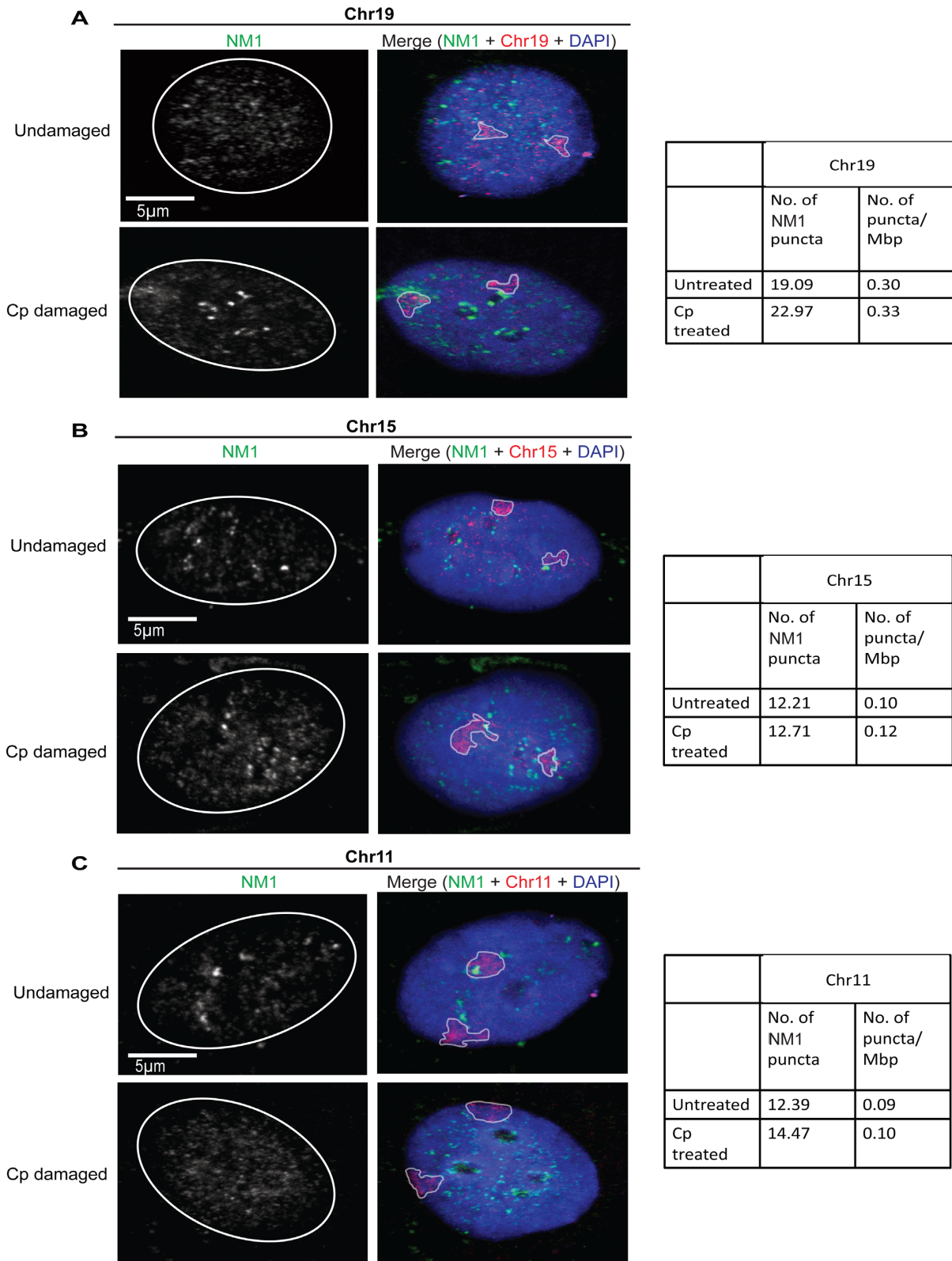
Figure 10. Analyses of NM1 levels in specific CTs by immuno-FISH. Representative images (100x magnification) of NHDF nuclei for NM1 Immuno-FISH, whereby staining for NM1 was combined with 3D-FISH for chromosomes (**A**) 19, (**B**) 15 and (**C**) 11. NM1 puncta on these CTs were counted in 3D confocal images using Imaris. Number of NM1 puncta were normalized to the chromosome length (Mbp). N = 2, n = at least 30 nuclei. NM1 Immuno-FISH revealed that NM1 puncta did not significantly increase on these CTs post cisplatin damage.

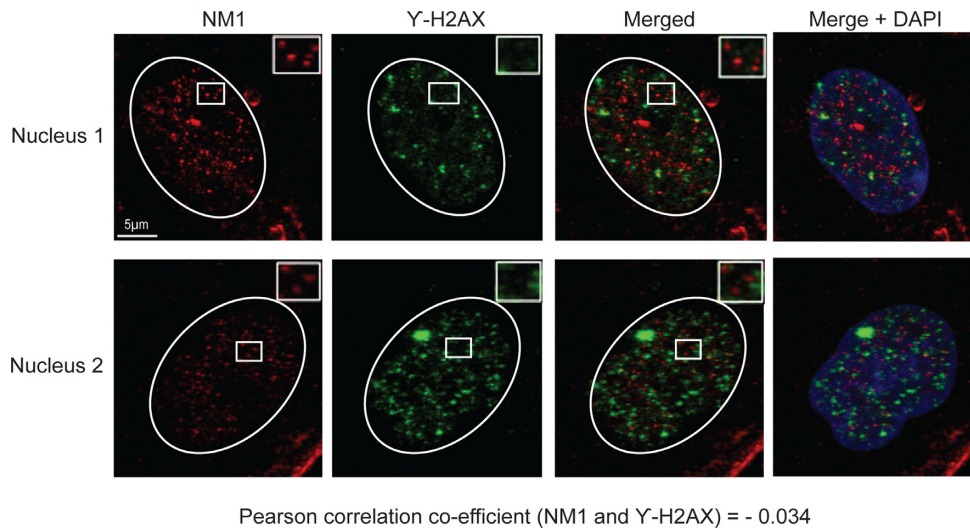Pearson correlation co-efficient (NM1 and Υ-H2AX) = - 0.034

Figure 11. NM1 does not co-localize with Υ-H2AX. 3D projections of confocal images taken at 100x magnification, showing no co-localization between Υ-H2AX (green) and NM1 (red) in cisplatin treated NHDFs**.** Co-localization analysis by computing the Pearson correlation co-efficient, was carried out in 3D images after background subtraction (to make the puncta more prominent) on at least 20 nuclei in 2 independent experiments using Imaris software.

ing DDR also needs to be interrogated in detail. It is likely that just as nuclear actin has been implicated in the functions of repair proteins such as SMARCAL1 (112), NM1 might engage in novel interactions specific to DDR. NM1 function during DDR poses certain fundamental mechanistic questions: Does DDR encompass specific post translational modification changes in NM1 leading to enhanced recruitment to chromatin? What is the role of ATPase motor function in NM1 *vis-à-vis* actin involvement in the damage induced CT relocation? All these questions remain open for detailed investigation as a part of a separate study.

In conclusion, our previous work (46) and the current results using cisplatin as a DNA damage inducer, shows that early sensing, repair and signaling at DSBs by ATM kinase, DNAPK and Υ-H2AX (Figure 3) seem to play an important role in DNA damage induced CT relocation. But when relatively later stages of DSB repair catalyzed by Rad51 or DNA ligase IV were blocked by using inhibitor or RNAi, damage induced CT relocation was only partially (CT 19) or not (CT 15) abrogated (Figure 4), indicating that later phases of repair do not seem to be as critical as the early phases of repair for orchestrating CT repositioning.

CT repositioning during serum starvation (40) and also the movement of a chromosomal domain (58) during transcriptional activation are thought to be mediated by nuclear motors such as actin and NM1. The functions of NM1 in the context of DDR are largely unknown. Our study for the first time delves into the involvement of NM1 in DDR in mammalian cells. In particular, we demonstrate that human fibroblasts are enriched with nuclear myosin that is tightly bound to chromatin (Figure 5A and B) and this association of NM1 to the chromatin is enhanced upon the induction of DNA damage using cisplatin or hydrogen peroxide-agents that lead to production of DNA DSBs during the DDR (Figure 5A), implying its functional relevance in DDR. This is further corroborated by two more lines of evidence: firstly, inhibition of upstream damage sensors such as ATM, ATR, DNAPK and PARP-1 led to the loss of DDR-associated

recruitment of NM1 (Figure 6) and secondly, down regulation of Υ-H2AX signaling itself also led to a concomitant loss in NM1 recruitment to chromatin (Figure 5C). We surmise that large-scale chromatin remodeling associated with multiple Υ-H2AX sites might trigger loading of DDR-induced NM1 on to chromatin. Indeed, siRNA mediated knockdown of NM1 levels or motor function defects in NM1 abrogated DNA damage induced CT relocation (Figures 7 and 8). NM1 has been implicated in relocation of CTs (40) as well as repositioning of a chromosomal domain (58). Our results in the current study are not only consistent with these findings, but are also an important step forward in understanding the mechanistic basis of NM1 recruitment to chromatin upon induction of DNA damage. We speculate that a co-ordination between early DDR sensing and signaling by ATM kinase, DNAPK and Υ-H2AX; subsequent chromatin remodeling and NM1 recruitment to the chromatin, is required for DNA damage induced CT relocation, which is an integral part of DDR. CT relocation perhaps is a means by which the cell orchestrates large-scale remodeling of nuclear milieu, thereby rewiring the transcriptional program to efficiently perform DDR in order to maintain its genomic stability.

SUPPLEMENTARY DATA

Supplementary Data are available at NAR Online.

ACKNOWLEDGEMENTS

REFERENCES

1. Lukas,J., Lukas,C. and Bartek,J. (2004) Mammalian cell cycle checkpoints: signalling pathways and their organization in space and time. *DNA Repair (Amst)*, **3**, 997–1007.
2. Malumbres,M. and Barbacid,M. (2009) Cell cycle, CDKs and cancer: a changing paradigm. *Nat. Rev. Cancer*, **9**, 153–166.
3. Kaina,B. (2003) DNA damage-triggered apoptosis: critical role of DNA repair, double-strand breaks, cell proliferation and signaling. *Biochem. Pharmacol.*, **66**, 1547–1554.
4. Roos,W.P. and Kaina,B. (2006) DNA damage-induced cell death by apoptosis. *Trends Mol. Med.*, **12**, 440–450.
5. Bassing,C.H. and Alt,F.W. (2004) The cellular response to general and programmed DNA double strand breaks. *DNA Repair (Amst)*, **3**, 781–796.
6. Sonoda,E., Hochegger,H., Saberi,A., Taniguchi,Y. and Takeda,S. (2006) Differential usage of non-homologous end-joining and homologous recombination in double strand break repair. *DNA Repair (Amst)*, **5**, 1021–1029.
7. Derheimer,F.A. and Kastan,M.B. (2010) Multiple roles of ATM in monitoring and maintaining DNA integrity. *FEBS Lett.*, **584**, 3675–3681.
8. Burma,S., Chen,B.P., Murphy,M., Kurimasa,A. and Chen,D.J. (2001) ATM phosphorylates histone H2AX in response to DNA double-strand breaks. *J. Biol. Chem.*, **276**, 42462–42467.
9. Rogakou,E.P., Pilch,D.R., Orr,A.H., Ivanova,V.S. and Bonner,W.M. (1998) DNA double-stranded breaks induce histone H2AX phosphorylation on serine 139. *J. Biol. Chem.*, **273**, 5858–5868.
10. Stiff,T., O'Driscoll,M., Rief,N., Iwabuchi,K., Lobrich,M. and Jeggo,P.A. (2004) ATM and DNA-PK function redundantly to phosphorylate H2AX after exposure to ionizing radiation. *Cancer Res.*, **64**, 2390–2396.
11. Lou,Z., Minter-Dykhouse,K., Franco,S., Gostissa,M., Rivera,M.A., Celeste,A., Manis,J.P., van Deursen,J., Nussenzweig,A., Paull,T.T. *et al.* (2006) MDC1 maintains genomic stability by participating in the amplification of ATM-dependent DNA damage signals. *Mol. Cell*, **21**, 187–200.
12. So,S., Davis,A.J. and Chen,D.J. (2009) Autophosphorylation at serine 1981 stabilizes ATM at DNA damage sites. *J. Cell Biol.*, **187**, 977–990.
13. Rogakou,E.P., Boon,C., Redon,C. and Bonner,W.M. (1999) Megabase chromatin domains involved in DNA double-strand breaks in vivo. *J. Cell Biol.*, **146**, 905–916.
14. Bekker-Jensen,S. and Mailand,N. (2010) Assembly and function of DNA double-strand break repair foci in mammalian cells. *DNA Repair (Amst)*, **9**, 1219–1228.
15. Kinner,A., Wu,W., Staudt,C. and Iliakis,G. (2008) Gamma-H2AX in recognition and signaling of DNA double-strand breaks in the context of chromatin. *Nucleic Acids Res.*, **36**, 5678–5694.
16. Downs,J.A., Allard,S., Jobin-Robitaille,O., Javaheri,A., Auger,A., Bouchard,N., Kron,S.J., Jackson,S.P. and Cote,J. (2004) Binding of chromatin-modifying activities to phosphorylated histone H2A at DNA damage sites. *Mol. Cell*, **16**, 979–990.
17. Morrison,A.J., Highland,J., Krogan,N.J., Arbel-Eden,A., Greenblatt,J.F., Haber,J.E. and Shen,X. (2004) INO80 and gamma-H2AX interaction links ATP-dependent chromatin remodeling to DNA damage repair. *Cell*, **119**, 767–775.
18. Thiriet,C. and Hayes,J.J. (2005) Chromatin in need of a fix: phosphorylation of H2AX connects chromatin to DNA repair. *Mol. Cell*, **18**, 617–622.
19. Celeste,A., Petersen,S., Romanienko,P.J., Fernandez-Capetillo,O., Chen,H.T., Sedelnikova,O.A., Reina-San-Martin,B., Coppola,V., Meffre,E., Difilippantonio,M.J. *et al.* (2002) Genomic instability in mice lacking histone H2AX. *Science*, **296**, 922–927.
20. Fernandez-Capetillo,O., Chen,H.T., Celeste,A., Ward,I., Romanienko,P.J., Morales,J.C., Naka,K., Xia,Z., Camerini-Otero,R.D., Motoyama,N. *et al.* (2002) DNA damage-induced G2-M checkpoint activation by histone H2AX and 53BP1. *Nat. Cell Biol.*, **4**, 993–997.
21. Fragkos,M., Jurvansuu,J. and Beard,P. (2009) H2AX is required for cell cycle arrest via the p53/p21 pathway. *Mol. Cell. Biol.*, **29**, 2828–2840.
22. Bassing,C.H., Chua,K.F., Sekiguchi,J., Suh,H., Whitlow,S.R., Fleming,J.C., Monroe,B.C., Ciccone,D.N., Yan,C., Vlasakova,K. *et al.* (2002) Increased ionizing radiation sensitivity and genomic instability in the absence of histone H2AX. *Proc. Natl. Acad. Sci. U.S.A.*, **99**, 8173–8178.
23. Ira,G. and Hastings,P.J. (2012) DNA breakage drives nuclear search. *Nat. Cell Biol.*, **14**, 448–450.
24. Mine-Hattab,J. and Rothstein,R. (2012) Increased chromosome mobility facilitates homology search during recombination. *Nat. Cell Biol.*, **14**, 510–517.
25. Dion,V., Kalck,V., Horigome,C., Towbin,B.D. and Gasser,S.M. (2012) Increased mobility of double-strand breaks requires Mec1, Rad9 and the homologous recombination machinery. *Nat. Cell Biol.*, **14**, 502–509.
26. Soutoglou,E., Dorn,J.F., Sengupta,K., Jasin,M., Nussenzweig,A., Ried,T., Danuser,G. and Misteli,T. (2007) Positional stability of single double-strand breaks in mammalian cells. *Nat. Cell Biol.*, **9**, 675–682.
27. Krawczyk,P.M., Borovski,T., Stap,J., Cijsouw,T., ten Cate,R., Medema,J.P., Kanaar,R., Franken,N.A. and Aten,J.A. (2012) Chromatin mobility is increased at sites of DNA double-strand breaks. *J. Cell Sci.*, **125**, 2127–2133.
28. Lisby,M., Mortensen,U.H. and Rothstein,R. (2003) Colocalization of multiple DNA double-strand breaks at a single Rad52 repair centre. *Nat. Cell Biol.*, **5**, 572–577.
29. Aten,J.A., Stap,J., Krawczyk,P.M., van Oven,C.H., Hoebe,R.A., Essers,J. and Kanaar,R. (2004) Dynamics of DNA double-strand breaks revealed by clustering of damaged chromosome domains. *Science*, **303**, 92–95.
30. Neumaier,T., Swenson,J., Pham,C., Polyzos,A., Lo,A.T., Yang,P., Dyball,J., Asaithamby,A., Chen,D.J., Bissell,M.J. *et al.* (2012) Evidence for formation of DNA repair centers and dose-response nonlinearity in human cells. *Proc. Natl. Acad. Sci. U.S.A.*, **109**, 443–448.
31. Misteli,T. and Soutoglou,E. (2009) The emerging role of nuclear architecture in DNA repair and genome maintenance. *Nat. Rev. Mol. Cell Biol.*, **10**, 243–254.
32. Cremer,T. and Cremer,C. (2001) Chromosome territories, nuclear architecture and gene regulation in mammalian cells. *Nat. Rev. Genet.*, **2**, 292–301.
33. Cremer,T., Cremer,M., Dietzel,S., Muller,S., Solovei,I. and Fakan,S. (2006) Chromosome territories–a functional nuclear landscape. *Curr. Opin. Cell Biol.*, **18**, 307–316.
34. Foster,H.A. and Bridger,J.M. (2005) The genome and the nucleus: a marriage made by evolution. Genome organisation and nuclear architecture. *Chromosoma*, **114**, 212–229.
35. Parada,L. and Misteli,T. (2002) Chromosome positioning in the interphase nucleus. *Trends Cell Biol.*, **12**, 425–432.
36. Neusser,M., Schubel,V., Koch,A., Cremer,T. and Muller,S. (2007) Evolutionarily conserved, cell type and species-specific higher order chromatin arrangements in interphase nuclei of primates. *Chromosoma*, **116**, 307–320.
37. Tanabe,H., Muller,S., Neusser,M., von Hase,J., Calcagno,E., Cremer,M., Solovei,I., Cremer,C. and Cremer,T. (2002) Evolutionary conservation of chromosome territory arrangements in cell nuclei from higher primates. *Proc. Natl. Acad. Sci. U.S.A.*, **99**, 4424–4429.
38. Boyle,S., Gilchrist,S., Bridger,J.M., Mahy,N.L., Ellis,J.A. and Bickmore,W.A. (2001) The spatial organization of human

chromosomes within the nuclei of normal and emerin-mutant cells. *Hum. Mol. Genet.*, **10**, 211–219.

39. Croft,J.A., Bridger,J.M., Boyle,S., Perry,P., Teague,P. and Bickmore,W.A. (1999) Differences in the localization and morphology of chromosomes in the human nucleus. *J. Cell Biol.*, **145**, 1119–1131.

40. Mehta,I.S., Amira,M., Harvey,A.J. and Bridger,J.M. (2010) Rapid chromosome territory relocation by nuclear motor activity in response to serum removal in primary human fibroblasts. *Genome Biol.*, **11**, R5.

41. Mehta,I.S., Eskiw,C.H., Arican,H.D., Kill,I.R. and Bridger,J.M. (2011) Farnesyltransferase inhibitor treatment restores chromosome territory positions and active chromosome dynamics in Hutchinson-Gilford progeria syndrome cells. *Genome Biol.*, **12**, R74.

42. Borden,J. and Manuelidis,L. (1988) Movement of the X chromosome in epilepsy. *Science*, **242**, 1687–1691.

43. Martou,G. and De Boni,U. (2000) Nuclear topology of murine, cerebellar Purkinje neurons: changes as a function of development. *Exp. Cell Res.*, **256**, 131–139.

44. Kuroda,M., Tanabe,H., Yoshida,K., Oikawa,K., Saito,A., Kiyuna,T., Mizusawa,H. and Mukai,K. (2004) Alteration of chromosome positioning during adipocyte differentiation. *J. Cell Sci.*, **117**, 5897–5903.

45. Krystosek,A. (1998) Repositioning of human interphase chromosomes by nucleolar dynamics in the reverse transformation of HT1080 fibrosarcoma cells. *Exp. Cell Res.*, **241**, 202–209.

46. Mehta,I.S., Kulashreshtha,M., Chakraborty,S., Kolthur-Seetharam,U. and Rao,B.J. (2013) Chromosome territories reposition during DNA damage-repair response. *Genome Biol.*, **14**, R135.

47. Frankenberg-Schwager,M., Kirchermeier,D., Greif,G., Baer,K., Becker,M. and Frankenberg,D. (2005) Cisplatin-mediated DNA double-strand breaks in replicating but not in quiescent cells of the yeast Saccharomyces cerevisiae. *Toxicology*, **212**, 175–184.

48. Huang,X., Okafuji,M., Traganos,F., Luther,E., Holden,E. and Darzynkiewicz,Z. (2004) Assessment of histone H2AX phosphorylation induced by DNA topoisomerase I and II inhibitors topotecan and mitoxantrone and by the DNA cross-linking agent cisplatin. *Cytometry A*, **58**, 99–110.

49. Kuo,L.J. and Yang,L.X. (2008) Gamma-H2AX - a novel biomarker for DNA double-strand breaks. *In Vivo*, **22**, 305–309.

50. Lloyd,D.R. and Phillips,D.H. (1999) Oxidative DNA damage mediated by copper(II), iron(II) and nickel(II) fenton reactions: evidence for site-specific mechanisms in the formation of double-strand breaks, 8-hydroxydeoxyguanosine and putative intrastrand cross-links. *Mutat. Res.*, **424**, 23–36.

51. Sorenson,C.M. and Eastman,A. (1988) Mechanism of cis-diamminedichloroplatinum(II)-induced cytotoxicity: role of G2 arrest and DNA double-strand breaks. *Cancer Res.*, **48**, 4484–4488.

52. Vock,E.H., Lutz,W.K., Hormes,P., Hoffmann,H.D. and Vamvakas,S. (1998) Discrimination between genotoxicity and cytotoxicity in the induction of DNA double-strand breaks in cells treated with etoposide, melphalan, cisplatin, potassium cyanide, Triton X-100, and gamma-irradiation. *Mutat. Res.*, **413**, 83–94.

53. Ward,J.F., Evans,J.W., Limoli,C.L. and Calabro-Jones,P.M. (1987) Radiation and hydrogen peroxide induced free radical damage to DNA. *Br. J. Cancer Suppl.*, **8**, 105–112.

54. Frankenberg-Schwager,M., Becker,M., Garg,I., Pralle,E., Wolf,H. and Frankenberg,D. (2008) The role of nonhomologous DNA end joining, conservative homologous recombination, and single-strand annealing in the cell cycle-dependent repair of DNA double-strand breaks induced by H(2)O(2) in mammalian cells. *Radiat. Res.*, **170**, 784–793.

55. Falk,M., Lukasova,E. and Kozubek,S. (2008) Chromatin structure influences the sensitivity of DNA to gamma-radiation. *Biochim. Biophys. Acta*, **1783**, 2398–2414.

56. Gazave,E., Gautier,P., Gilchrist,S. and Bickmore,W.A. (2005) Does radial nuclear organisation influence DNA damage? *Chromosome Res.*, **13**, 377–388.

57. Dundr,M., Ospina,J.K., Sung,M.H., John,S., Upender,M., Ried,T., Hager,G.L. and Matera,A.G. (2007) Actin-dependent intranuclear repositioning of an active gene locus in vivo. *J. Cell Biol.*, **179**, 1095–1103.

58. Chuang,C.H., Carpenter,A.E., Fuchsova,B., Johnson,T., de Lanerolle,P. and Belmont,A.S. (2006) Long-range directional movement of an interphase chromosome site. *Curr. Biol.*, **16**, 825–831.

59. Dzijak,R., Yildirim,S., Kahle,M., Novak,P., Hnilicova,J., Venit,T. and Hozak,P. (2012) Specific nuclear localizing sequence directs two myosin isoforms to the cell nucleus in calmodulin-sensitive manner. *PloS One*, **7**, e30529.

60. Ihnatovych,I., Migocka-Patrzalek,M., Dukh,M. and Hofmann,W.A. (2012) Identification and characterization of a novel myosin Ic isoform that localizes to the nucleus. *Cytoskeleton (Hoboken)*, **69**, 555–565.

61. Ihnatovych,I., Sielski,N.L. and Hofmann,W.A. (2014) Selective expression of myosin IC Isoform A in mouse and human cell lines and mouse prostate cancer tissues. *PLoS One*, **9**, e108609.

62. Venit,T., Dzijak,R., Kalendova,A., Kahle,M., Rohozkova,J., Schmidt,V., Rulicke,T., Rathkolb,B., Hans,W., Bohla,A. *et al.* (2013) Mouse nuclear myosin I knock-out shows interchangeability and redundancy of myosin isoforms in the cell nucleus. *PLoS One*, **8**, e61406.

63. Pestic-Dragovich,L., Stojiljkovic,L., Philimonenko,A.A., Nowak,G., Ke,Y., Settlage,R.E., Shabanowitz,J., Hunt,D.F., Hozak,P. and de Lanerolle,P. (2000) A myosin I isoform in the nucleus. *Science*, **290**, 337–341.

64. Percipalle,P., Fomproix,N., Cavellan,E., Voit,R., Reimer,G., Kruger,T., Thyberg,J., Scheer,U., Grummt,I. and Farrants,A.K. (2006) The chromatin remodelling complex WSTF-SNF2h interacts with nuclear myosin 1 and has a role in RNA polymerase I transcription. *EMBO Rep.*, **7**, 525–530.

65. Philimonenko,V.V., Zhao,J., Iben,S., Dingova,H., Kysela,K., Kahle,M., Zentgraf,H., Hofmann,W.A., de Lanerolle,P., Hozak,P. *et al.* (2004) Nuclear actin and myosin I are required for RNA polymerase I transcription. *Nat. Cell Biol.*, **6**, 1165–1172.

66. Ye,J., Zhao,J., Hoffmann-Rohrer,U. and Grummt,I. (2008) Nuclear myosin I acts in concert with polymeric actin to drive RNA polymerase I transcription. *Genes Dev.*, **22**, 322–330.

67. Hofmann,W.A., Stojiljkovic,L., Fuchsova,B., Vargas,G.M., Mavrommatis,E., Philimonenko,V., Kysela,K., Goodrich,J.A., Lessard,J.L., Hope,T.J. *et al.* (2004) Actin is part of pre-initiation complexes and is necessary for transcription by RNA polymerase II. *Nat. Cell Biol.*, **6**, 1094–1101.

68. Hofmann,W.A., Vargas,G.M., Ramchandran,R., Stojiljkovic,L., Goodrich,J.A. and de Lanerolle,P. (2006) Nuclear myosin I is necessary for the formation of the first phosphodiester bond during transcription initiation by RNA polymerase II. *J. Cell. Biochem.*, **99**, 1001–1009.

69. Sarshad,A., Sadeghifar,F., Louvet,E., Mori,R., Bohm,S., Al-Muzzaini,B., Vintermist,A., Fomproix,N., Ostlund,A.K. and Percipalle,P. (2013) Nuclear myosin 1c facilitates the chromatin modifications required to activate rRNA gene transcription and cell cycle progression. *PLoS Genet.*, **9**, e1003397.

70. Almuzzaini,B., Sarshad,A.A., Farrants,A.K. and Percipalle,P. (2015) Nuclear myosin 1 contributes to a chromatin landscape compatible with RNA polymerase II transcription activation. *BMC Biol.*, **13**, 35.

71. Sarshad,A.A. and Percipalle,P. (2014) New insight into role of myosin motors for activation of RNA polymerases. *Int. Rev. Cell Mol. Biol.*, **311**, 183–230.

72. Fomproix,N. and Percipalle,P. (2004) An actin-myosin complex on actively transcribing genes. *Exp. Cell Res.*, **294**, 140–148.

73. Sarshad,A.A., Corcoran,M., Al-Muzzaini,B., Borgonovo-Brandter,L., Von Euler,A., Lamont,D., Visa,N. and Percipalle,P. (2014) Glycogen synthase kinase (GSK) 3beta phosphorylates and protects nuclear myosin 1c from proteasome-mediated degradation to activate rDNA transcription in early G1 cells. *PLoS Genet.*, **10**, e1004390.

74. Yang,X., Yu,W., Shi,L., Sun,L., Liang,J., Yi,X., Li,Q., Zhang,Y., Yang,F., Han,X. *et al.* (2011) HAT4, a Golgi apparatus-anchored B-type histone acetyltransferase, acetylates free histone H4 and facilitates chromatin assembly. *Mol. Cell*, **44**, 39–50.

75. Solovei,I. and Cremer,M. (2010) 3D-FISH on cultured cells combined with immunostaining. *Methods Mol. Biol.*, **659**, 117–126.

76. Chakraborty,S., Mehta,I., Kulashreshtha,M. and Rao,B.J. (2015) Quantitative analysis of chromosome localization in the nucleus. *Methods Mol. Biol.*, **1228**, 223–233.

77. Mehta,I., Chakraborty,S. and Rao,B.J. (2013) IMACULAT - an open access package for the quantitative analysis of chromosome localization in the nucleus. *PLoS One*, **8**, e61386.

78. Mendez,J. and Stillman,B. (2000) Chromatin association of human origin recognition complex, cdc6, and minichromosome maintenance proteins during the cell cycle: assembly of prereplication complexes in late mitosis. *Mol. Cell. Biol.*, **20**, 8602–8612.

79. Eaton,S.L., Roche,S.L., Llavero Hurtado,M., Oldknow,K.J., Farquharson,C., Gillingwater,T.H. and Wishart,T.M. (2013) Total protein analysis as a reliable loading control for quantitative fluorescent Western blotting. *PLoS One*, **8**, e72457.

80. Casanovas,O., Jaumot,M., Paules,A.B., Agell,N. and Bachs,O. (2004) P38SAPK2 phosphorylates cyclin D3 at Thr-283 and targets it for proteasomal degradation. *Oncogene*, **23**, 7537–7544.

81. Welinder,C. and Ekblad,L. (2011) Coomassie staining as loading control in Western blot analysis. *J. Proteome Res.*, **10**, 1416–1419.

82. Croft,D.R., Coleman,M.L., Li,S., Robertson,D., Sullivan,T., Stewart,C.L. and Olson,M.F. (2005) Actin-myosin-based contraction is responsible for apoptotic nuclear disintegration. *J. Cell Biol.*, **168**, 245–255.

83. Tone,S., Sugimoto,K., Tanda,K., Suda,T., Uehira,K., Kanouchi,H., Samejima,K., Minatogawa,Y. and Earnshaw,W.C. (2007) Three distinct stages of apoptotic nuclear condensation revealed by time-lapse imaging, biochemical and electron microscopy analysis of cell-free apoptosis. *Exp. Cell Res.*, **313**, 3635–3644.

84. Anderson,L., Henderson,C. and Adachi,Y. (2001) Phosphorylation and rapid relocalization of 53BP1 to nuclear foci upon DNA damage. *Mol. Cell. Biol.*, **21**, 1719–1729.

85. Fink,L.S., Roell,M., Caiazza,E., Lerner,C., Stamato,T., Hrelia,S., Lorenzini,A. and Sell,C. (2011) 53BP1 contributes to a robust genomic stability in human fibroblasts. *Aging*, **3**, 836–845.

86. Ward,I.M., Minn,K., Jorda,K.G. and Chen,J. (2003) Accumulation of checkpoint protein 53BP1 at DNA breaks involves its binding to phosphorylated histone H2AX. *J. Biol. Chem.*, **278**, 19579–19582.

87. Harding,S.M. and Bristow,R.G. (2012) Discordance between phosphorylation and recruitment of 53BP1 in response to DNA double-strand breaks. *Cell Cycle*, **11**, 1432–1444.

88. Miller,K.M., Tjeertes,J.V., Coates,J., Legube,G., Polo,S.E., Britton,S. and Jackson,S.P. (2010) Human HDAC1 and HDAC2 function in the DNA-damage response to promote DNA nonhomologous end-joining. *Nat. Struct. Mol. Biol.*, **17**, 1144–1151.

89. van Attikum,H., Fritsch,O., Hohn,B. and Gasser,S.M. (2004) Recruitment of the INO80 complex by H2A phosphorylation links ATP-dependent chromatin remodeling with DNA double-strand break repair. *Cell*, **119**, 777–788.

90. Thompson,L.H. and Schild,D. (2001) Homologous recombinational repair of DNA ensures mammalian chromosome stability. *Mutat. Res.*, **477**, 131–153.

91. Henning,W. and Sturzbecher,H.W. (2003) Homologous recombination and cell cycle checkpoints: Rad51 in tumour progression and therapy resistance. *Toxicology*, **193**, 91–109.

92. Wilson,T.E., Grawunder,U. and Lieber,M.R. (1997) Yeast DNA ligase IV mediates non-homologous DNA end joining. *Nature*, **388**, 495–498.

93. Wang,H., Zeng,Z.C., Perrault,A.R., Cheng,X., Qin,W. and Iliakis,G. (2001) Genetic evidence for the involvement of DNA ligase IV in the DNA-PK-dependent pathway of non-homologous end joining in mammalian cells. *Nucleic Acids Res.*, **29**, 1653–1660.

94. Srivastava,M., Nambiar,M., Sharma,S., Karki,S.S., Goldsmith,G., Hegde,M., Kumar,S., Pandey,M., Singh,R.K., Ray,P. *et al.* (2012) An inhibitor of nonhomologous end-joining abrogates double-strand break repair and impedes cancer progression. *Cell*, **151**, 1474–1487.

95. Maruyama,T., Dougan,S.K., Truttmann,M.C., Bilate,A.M., Ingram,J.R. and Ploegh,H.L. (2015) Increasing the efficiency of precise genome editing with CRISPR-Cas9 by inhibition of nonhomologous end joining. *Nat. Biotechnol.*, **33**, 538–542.

96. Chu,V.T., Weber,T., Wefers,B., Wurst,W., Sander,S., Rajewsky,K. and Kuhn,R. (2015) Increasing the efficiency of homology-directed repair for CRISPR-Cas9-induced precise gene editing in mammalian cells. *Nat. Biotechnol.*, **33**, 543–548.

97. Hofmann,W.A., Johnson,T., Klapczynski,M., Fan,J.L. and de Lanerolle,P. (2006) From transcription to transport: emerging roles for nuclear myosin I. *Biochem. Cell Biol.*, **84**, 418–426.

98. Katyal,S., Lee,Y., Nitiss,K.C., Downing,S.M., Li,Y., Shimada,M., Zhao,J., Russell,H.R., Petrini,J.H., Nitiss,J.L. *et al.* (2014) Aberrant topoisomerase-1 DNA lesions are pathogenic in neurodegenerative genome instability syndromes. *Nat. Neurosci.*, **17**, 813–821.

99. Shanbhag,N.M. and Greenberg,R.A. (2010) Neighborly DISCourse: DNA double strand breaks silence transcription. *Cell Cycle*, **9**, 3635–3636.

100. Moon,S.H., Lin,L., Zhang,X., Nguyen,T.A., Darlington,Y., Waldman,A.S., Lu,X. and Donehower,L.A. (2010) Wild-type p53-induced phosphatase 1 dephosphorylates histone variant gamma-H2AX and suppresses DNA double strand break repair. *J. Biol. Chem.*, **285**, 12935–12947.

101. Ryves,W.J. and Harwood,A.J. (2001) Lithium inhibits glycogen synthase kinase-3 by competition for magnesium. *Biochem. Biophys. Res. Commun.*, **280**, 720–725.

102. Kramer,T., Schmidt,B. and Lo Monte,F. (2012) Small-molecule inhibitors of GSK-3: Structural insights and their application to Alzheimer's disease models. *Int. J. Alzheimer's Dis.*, **2012**, 381029.

103. George,B., Vollenbroker,B., Saleem,M.A., Huber,T.B., Pavenstadt,H. and Weide,T. (2011) GSK3beta inactivation in podocytes results in decreased phosphorylation of p70S6K accompanied by cytoskeletal rearrangements and inhibited motility. *Am. J. Physiol. Renal Physiol.*, **300**, F1152–F1162.

104. De Sarno,P., Li,X. and Jope,R.S. (2002) Regulation of Akt and glycogen synthase kinase-3 beta phosphorylation by sodium valproate and lithium. *Neuropharmacology*, **43**, 1158–1164.

105. Li,X., Friedman,A.B., Zhu,W., Wang,L., Boswell,S., May,R.S., Davis,L.L. and Jope,R.S. (2007) Lithium regulates glycogen synthase kinase-3beta in human peripheral blood mononuclear cells: implication in the treatment of bipolar disorder. *Biol. Psychiatry*, **61**, 216–222.

106. Alao,J.P., Stavropoulou,A.V., Lam,E.W. and Coombes,R.C. (2006) Role of glycogen synthase kinase 3 beta (GSK3beta) in mediating the cytotoxic effects of the histone deacetylase inhibitor trichostatin A (TSA) in MCF-7 breast cancer cells. *Mol. Cancer*, **5**, 40.

107. Zhang,F., Phiel,C.J., Spece,L., Gurvich,N. and Klein,P.S. (2003) Inhibitory phosphorylation of glycogen synthase kinase-3 (GSK-3) in response to lithium. Evidence for autoregulation of GSK-3. *J. Biol. Chem.*, **278**, 33067–33077.

108. Mone,M.J., Volker,M., Nikaido,O., Mullenders,L.H., van Zeeland,A.A., Verschure,P.J., Manders,E.M. and van Driel,R. (2001) Local UV-induced DNA damage in cell nuclei results in local transcription inhibition. *EMBO Rep.*, **2**, 1013–1017.

109. Seiler,D.M., Rouquette,J., Schmid,V.J., Strickfaden,H., Ottmann,C., Drexler,G.A., Mazurek,B., Greubel,C., Hable,V., Dollinger,G. *et al.* (2011) Double-strand break-induced transcriptional silencing is associated with loss of tri-methylation at H3K4. *Chromosome Res.*, **19**, 883–899.

110. Shanbhag,N.M., Rafalska-Metcalf,I.U., Balane-Bolivar,C., Janicki,S.M. and Greenberg,R.A. (2010) ATM-dependent chromatin changes silence transcription in cis to DNA double-strand breaks. *Cell*, **141**, 970–981.

111. Solovjeva,L.V., Svetlova,M.P., Chagin,V.O. and Tomilin,N.V. (2007) Inhibition of transcription at radiation-induced nuclear foci of phosphorylated histone H2AX in mammalian cells. *Chromosome Res.*, **15**, 787–797.

112. Feldkamp,M.D., Mason,A.C., Eichman,B.F. and Chazin,W.J. (2014) Structural analysis of replication protein A recruitment of the DNA damage response protein SMARCAL1. *Biochemistry*, **53**, 3052–3061.

113. Spitzer,M., Wildenhain,J., Rappsilber,J. and Tyers,M. (2014) BoxPlotR: a web tool for generation of box plots. *Nat. Methods*, **11**, 121–122.